Chemical Geology 662 (2024) 122229

Contents lists available at ScienceDirect

Chemical Geology

journal homepage: www.elsevier.com/locate/chemgeo

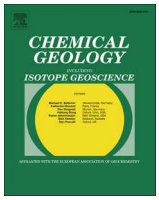

Sources of limestone dissolution from surface water-groundwater interaction in the carbonate critical zone

Andrew Oberhelman [a,*], Jonathan B. Martin [b], Madison K. Flint [b]

[a] Department of Earth and Environment, Florida International University, 11200 SW 8th Street, AHC5 360, Miami, FL 33199, USA
[b] Department of Geological Sciences, University of Florida, 241 Williamson Hall, PO Box 112120, Gainesville, FL 32611-2120, USA

ARTICLE INFO

Editor: Karen Johannesson

Keywords:
Surface water-groundwater interactions
Carbonate dissolution
Redox
Critical zone
Carbon cycle

ABSTRACT

Dissolution of carbonate minerals in karst aquifers has long been recognized to result from recharge of surface water undersaturated with respect to calcite from carbonic acid produced by hydration of dissolved atmospheric and respired CO_2. However, dissolution also results from additional acids produced by reactions of redox sensitive solutes in the subsurface, which may represent a source of CO_2 to Earth's atmosphere. Because the magnitude of dissolution by these additional acids is poorly constrained, we compare here fractions of dissolution from initial surface water undersaturation and subsurface redox reactions. Estimates are based on chemical mixing and geochemical (PHREEQC) modeling of time series measurements of water compositions at a spring vent that receives surface water during stream flooding and a stream sink-rise system in north-central Florida. During a single spring reversal, 9.2×10^5 kg of limestone dissolved. At the stream sink-rise system, where subsurface residence times are shorter than during the spring reversal, both limestone dissolution (10^2–10^4 kg) and precipitation (10^2–10^5 kg) occur as water flows through the conduits with residence times ranging from 10 to 70 h. At both sites, maximum calcite dissolution rates of ~10 μM hr^{-1} occurs at subsurface residence times between 30 and 50 h. For subsurface residence time > ~20–60 h, the models indicate that production of additional acid in the subsurface is required for ~53 ± 7% of dissolution. Oxidation of organic carbon, ammonium, pyrite, iron, and/or manganese produce sufficient acid for additional dissolution, but dissolved oxygen is insufficient for these reactions, indicating some acidity is generated under anerobic conditions. Dissolution caused by subsurface reactions in our samples represents mobilization of 20×10^4-30×10^4 kg of CO_2 via remineralization of organic carbon or carbonate dissolution by nitric and sulfuric acids. Acid produced by subsurface redox reactions during surface water-groundwater interactions, including non-carbonic acids, are important in conduit development and carbon cycling in the carbonate critical zone.

1. Introduction

Dissolution of soluble minerals, mainly carbonates, in karst landscapes is dominated by carbonic acid (H_2CO_3) generated by the hydration of dissolved atmospheric and respired CO_2 (Gulley et al., 2016, 2020). Carbonate mineral dissolution is congruent, which creates groundwater flow systems dominated by interconnected secondary voids. Secondary voids can be air- or water-filled and may be sufficiently large for human exploration. Additional features and phenomena resulting from dissolution include dolines, limestone pavement, speleothems, air-filled caves, water-filled conduits, and streams that sink into aquifer systems, thereby providing point recharge of water undersaturated with respect to carbonate minerals (Klimchouk, 2016; Ford and Williams, 2007). This point recharge has important implications for both the availability and contamination of water resources as well as for changing the architecture of the carbonate critical zone (Covington et al., 2023).

Acids in addition to carbonic acid, notably sulfuric and nitric acids, also contribute to carbonate mineral dissolution (Martin, 2017; Klimchouk, 2016; Torres et al., 2014; Perrin et al., 2008). In catchments impaired by acid rain and N fertilizers, sulfuric and nitric acids are estimated to cause between 3 and 60% of carbonate weathering and have increased carbonate weathering rates by ~20% (He et al., 2022; Xie et al., 2021; Zhang et al., 2020; Huang et al., 2017; Li et al., 2008). Additionally, in hypogenic karst systems, where upwelling water is commonly enriched in reduced sulfur, sulfuric acid drives most of the

* Corresponding author.
E-mail address: aoberhel@fiu.edu (A. Oberhelman).

https://doi.org/10.1016/j.chemgeo.2024.122229
Received 4 March 2024; Received in revised form 8 June 2024; Accepted 12 June 2024
Available online 13 June 2024

dissolution (Jones et al., 2012, 2014, 2015; Engel et al., 2004). Thus, hypogene dissolution is independent of surface recharge and atmospheric CO_2 although it can form nascent conduits that evolve into epigenic karst with interaction of surface water and groundwater (Engel et al., 2004). Unlike hydration of dissolved atmospheric CO_2, concentrations of additional acids in the subsurface of epigene karst systems depend on the redox state of the groundwater, which commonly is controlled by organic matter oxidation. However, other electron donors and acceptors can contribute to the redox state, and potential acid formation, particularly in anoxic settings.

Although dissolution by acids other than carbonic has previously been recognized (Martin, 2017; Torres et al., 2014; Perrin et al., 2008), the magnitudes of acids produced and their contributions to dissolution in the subsurface during surface water-groundwater interactions are poorly constrained within the carbonate critical zone. Nonetheless, dissolution caused by each acid is critical to understanding the evolution of karst systems, potential impacts on water resources, and interactions with the global carbon cycle. Links between the global carbon cycle and the carbonate critical zone are important because carbonate landscapes represent the largest reservoir of carbon on Earth's surface (Falkowski et al., 2000). Specifically, dissolution by carbonic acid originating from atmospheric CO_2 represents an atmospheric sink over short timescales, although it is net neutral over geologic timescales (e.g., Walker et al., 1981; Berner et al., 1983), while carbonate mineral dissolution by non-carbonic acids (e.g., sulfuric and nitric) provides a source of CO_2 to the atmosphere (Martin, 2017; Guo et al., 2015; Torres et al., 2014; Beaulieu et al., 2011; Perrin et al., 2008; Anderson et al., 2000).

Various mechanisms create acids that contribute to carbonate mineral dissolution in addition to hydration of atmospheric CO_2 (Table 1). Microbial and root respiration may increase the partial pressure of CO_2 (pCO_2) in the vadose zone above atmospheric concentrations and contribute additional carbonic acid-driven dissolution (Gulley et al., 2020; Gulley et al., 2016; Gulley et al., 2015; Gulley et al., 2014; Cooper et al., 2016; Mattey et al., 2016; Whitaker and Smart, 2007; Baldini et al., 2006; Wood, 1985). Organic acids, in particular humic and fulvic acids, produced from the breakdown of plant and soil organic matter or secreted by roots contribute acidity that may cause carbonate dissolution, although their contribution in thought to be minor (Hessen and Tranvik, 1998; Ford and Williams, 2007). Sulfuric acid is produced where minerals or species containing reduced sulfur, such as pyrite or hydrogen sulfide, react with oxygen. Nitrification, the microbial oxidation of ammonium (NH_4^+) to nitrate (NO_3^-), produces nitric acid from oxidation of free NH_4^+ or the organic nitrogen associated with dissolved organic matter (DOM) (Gao et al., 2023; Stein, 2011). Nitric acid production has increased recently with the accumulation of reactive nitrogen species from widespread use of anthropogenic nitrogen fertilizers in aqueous systems including the carbonate critical zone (Erisman et al., 2008; Galloway et al., 2008; Newton et al., 1996). Fossil fuel usage represents another important anthropogenic source of both sulfuric and nitric acids that are deposited on the landscape as acid rain (Irwin and Williams, 1988). Although less widely reported as a source of dissolution, oxidation of reduced metal species like manganese(II) and iron(II) and precipitation of their highly insoluble oxyhydroxides also produces acids that depend on redox state (Matocha et al., 2012; Cravotta, 1993; Hem, 1981).

Table 1
Stoichiometry of aerobic acid-producing redox reactions.

Eq. #	Reaction Name	Chemical Reaction
Eq. (1)	DOM oxidation	$(CH_2O)_{106}(NH_3)_{16}H_3PO_4 + 138O_2 \rightarrow 106CO_2 + 122H_2O + 16NO_3^- + HPO_4^{2-} + 18H^+$
Eq. (2)	Pyrite Oxidation	$4FeS_2 + 15O_2 + 8H_2O \rightarrow 2Fe_2O_3 + 8SO_4^{2-} + 16H^+$
Eq. (3)	Nitrification	$NH_4^+ + 2O_2 \rightarrow NO_3^- + H_2O + 2H+$
Eq. (4)	Iron(II) Oxidation	$Fe^{2+} + 2O_2 + 2.5H_2O \rightarrow Fe(OH)_3 + 2H^+$
Eq. (5)	Manganese(II) Oxidation	$Mn^{2+} + 0.5O_2 + H_2O \rightarrow MnO_2 + 2H^+$

Surface water-groundwater interactions lead to variations in redox conditions of epigenetic karst aquifers that may be responsible for acid production (Table 1) and dissolution as surface water recharging karst aquifers provides redox sensitive solutes such as organic carbon, nutrients, metals, and oxygen to the subsurface (Brown et al., 2019; Kipper, 2019; Brown et al., 2014; Gulley et al., 2013b; Gulley et al., 2011; Bailly-Comte et al., 2010). Given the potential for variable kinetics of redox and dissolution reactions (e.g., Oberhelman et al., 2024), the length of time that the surface water resides in the subsurface may be a key control on the degree to which subsurface reactions contribute to dissolution. A primary goal of this work is to evaluate the role of subsurface residence time for recharge surface water in dissolution caused by subsurface redox reactions.

In this study, we separate relative contributions to dissolution from recharge of undersaturated surface water and acid-producing subsurface redox reactions (Table 1). We separate contributions with chemical mixing and thermodynamic geochemical (PHREEQC) models and the chemistry of water samples collected from study sites in north-central Florida, USA. The sites include a stream sink-rise system and springs that periodically receive surface water during stream flooding, including time-series sampling of one flooding event. Water that flows to the aquifer at the sinking stream remains in the aquifer for times ranging from less than a day to about a week while surface water that flows into the spring during flooding events can reside in the subsurface for more than a month. These variations in subsurface residence times allow evaluation of rates of reactions (Oberhelman et al., 2024). We test the hypotheses that the subsurface residence time of intruding surface water will control the magnitude of dissolution caused by acids derived from various subsurface redox reactions and that there is a threshold subsurface residence time beyond which additional acid produced by redox reactions will be required for dissolution.

2. Methods

2.1. Study location

The study location is in the Suwannee River watershed in north-central Florida, USA (Fig. 1). The watershed is underlain by the karstic Floridan aquifer, which consists of pre-Miocene eogenetic carbonate rocks. The aquifer is confined in the northern portion by Miocene Hawthorn Group siliciclastic rocks and unconfined in the southern portion. A middle confining unit separates the Floridan aquifer into the upper Floridan aquifer (UFA) and the Lower Floridan aquifer. The UFA is composed of the Oligocene Suwannee and Eocene Ocala limestones and has porosities and matrix permeabilities around 30% and 10^{-13} m^2, respectively (Budd and Vacher, 2004). Ocala Limestone is >95% calcite by weight with trace amounts of clay, organics, and dolomite (Schmidt et al., 1979). Suwannee Limestone is less pure with greater amounts of silica and is only present at one of our sample locations (Madison Blue Spring) (Williams and Kuniansky, 2015; Schmidt et al., 1979). Pyrite is a minor constituent of both Ocala and Suwannee limestones, although greater amounts occur in the Suwannee Limestone (Pichler et al., 2011; Price and Pichler, 2006). The Hawthorn Group, which reaches a maximum thickness in north-central Florida of 95 m, has been removed by erosion in the southwestern region of the Suwannee River watershed. The boundary between confined and unconfined UFA forms a geomorphic feature called the Cody Scarp (−Scott, 1988). Where the Floridan aquifer is confined, abundant surface water features form, including lakes and streams. Where the Floridan aquifer is unconfined, surface water is limited to the Suwannee River, its major tributary, the Santa Fe River, and small spring runs draining to both rivers.

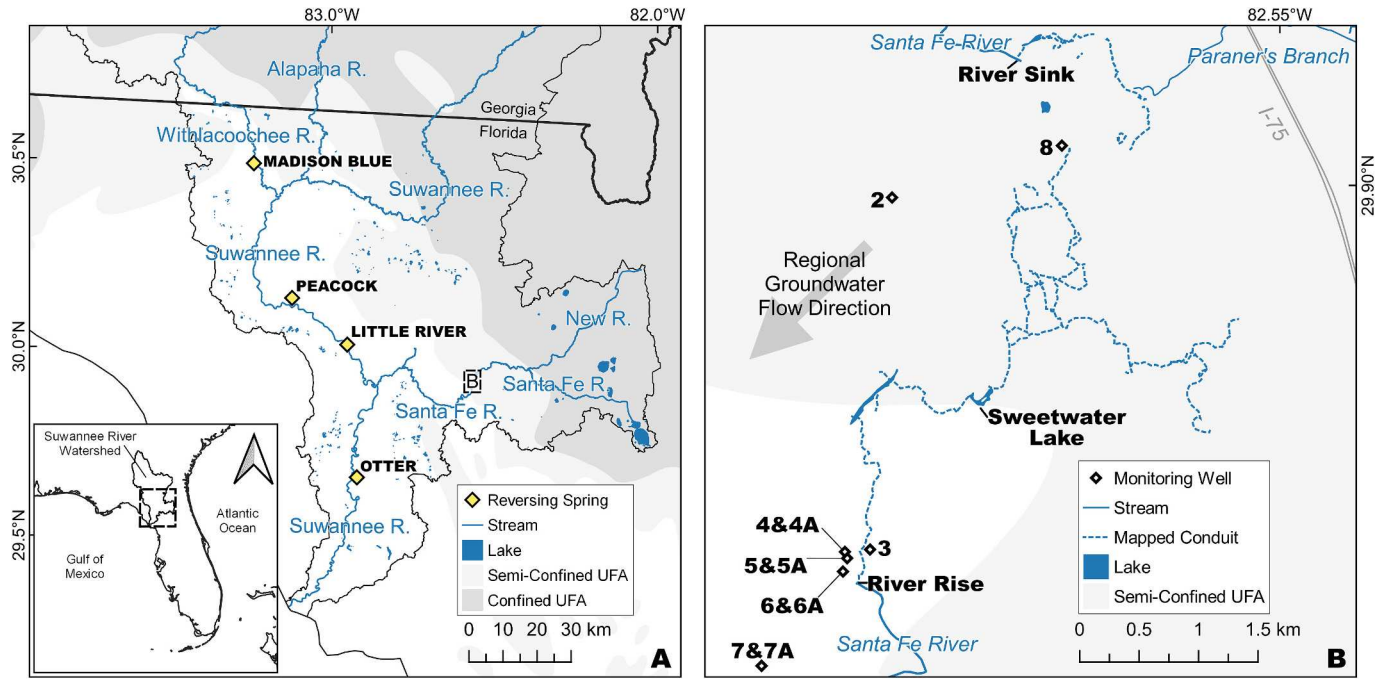

Fig. 1. Maps of the study area and sample sites in north-central Florida. (**A**) Suwanee River watershed showing the major drainages, sampled reversing springs, the Sink-Rise system outlined by the dashed box shown in panel B, and the Cody Scarp, which is roughly represented by the semi-confined UFA. (**B**) Map of the Santa Fe River Sink-Rise system showing River Sink, Sweetwater Lake, River Rise, mapped conduit, and monitoring well locations. Monitoring well sites that contain a clustered shallow well are labeled with a second number containing an 'A'.

2.2. Sampling locations

Samples were collected across north-central Florida, USA, including from Madison Blue Spring, Peacock Springs, Little River Spring, and Otter Spring, and at various locations of the Santa Fe River where it flows into the subsurface at a sinkhole and reemerges at a first-magnitude spring south of the sinkhole (a region referred to herein as the Sink-Rise system), (Fig. 1). Groundwater samples were also collected from wells at the Sink-Rise system and compared with legacy data from Floridan aquifer public supply wells that span all of Florida and into southern Georgia (McMahon et al., 2017). All sample locations have similar aquifer characteristics and semi-tropical climatic conditions because of their geographic proximity.

Madison Blue Spring, Otter Spring, Little River Spring, and Peacock Spring are classified as 1st (Madison Blue), 2nd (Otter and Little River), or 3rd (Peacock) magnitude with discharges of ≥2.8, 0.28–2.8, and 0.03–0.28 m^3/s, respectively (e.g., Meinzer, 1927). They discharge water to short spring runs (less than a few hundred meters) that flow to the Withlacoochee or Suwannee rivers. Because of the short spring runs and flat regional topography, flooding of the receiving rivers reverse the flow direction of the spring run, allowing river water to flow into the spring vent. These periods of reversed flow alter spring water chemistry, which at baseflow is largely invariant, for weeks to months after discharge resumes (e.g., Gulley et al., 2011; Flint et al., 2021). During flood recessions, discharging water from Madison Blue Spring is a mixture of the recently recharged river water, which resides in the subsurface for periods of weeks to months (Oberhelman et al., 2024), and groundwater that discharges during spring baseflow, which has subsurface residence times on the order of decades (Katz et al., 2001). We use the term 'recharge phase' to describe the period of a reversal when river water is flowing into the spring vent and the term 'recession phase' to describe the period where the spring is discharging mixed river water and groundwater as baseflow conditions reestablish.

Where the Santa Fe River crosses the Cody Scarp, it flows into a ~ 36 m deep sinkhole (River Sink), which captures the entire river flow, except during extreme floods when a small fraction of the river flows across the land surface. In the subsurface, water flows through partially mapped anastomosing water-filled conduits that connect River Sink with River Rise, a first magnitude spring ~8 km to the south that represents the headwaters of the lower Santa Fe River. The conduits connecting River Sink to River Rise have several collapse sinkholes that provide connections from the conduits to the surface, one of which, Sweetwater Lake, was sampled for this project (Fig. 1B). Gain or loss of water from the conduits is identified by the difference in river discharge measured at River Sink and River Rise, with losing conditions common during floods when flow captured by River Sink exceeds River Rise discharge (Martin et al., 2006; Bailly-Comte et al., 2010). Seven groundwater monitoring well sites are located near the mapped location of Sink-Rise system conduits. Four of these sites contain clustered deep and shallow wells. All wells are cased with 5.1 cm diameter PVC casing, with shallow wells extending to the water table (~1–3 m below land surface) and deep wells to the depth of the conduits (~30 m below land surface) (Ritorto et al., 2009). The shallow wells have a 3 m screened interval and the deep wells have a 6 m screened interval at their base.

During 2018–2020 and 2022, a total of 174 samples were collected at variable frequencies. During 2021, the Sink-Rise system was sampled biweekly (Fig. 2) and the reversing springs were sampled every three months. Madison Blue Spring reverses on average once or twice per year. One reversal was sampled between mid-February and mid-April 2021, at an average rate of 1 sample every 4 days, with greater frequency during the recession phase of the reversal (Fig. 3). Wells were sampled at least twice during 2020–2021. Exact sample dates and times are listed in the accompanying data set (Oberhelman et al., 2023a).

2.3. Field and laboratory methods

Water was pumped from spring vents, River Sink, Sweetwater Lake, and River Rise using a Geotech peristaltic pump and weighted PVC tubing inserted into the water body. The pump outlet was connected to an overflow cup where a YSI ProQuatro Multiparameter Meter was used to monitor temperature, dissolved oxygen (DO), specific conductivity, and pH until values stabilized and were recorded, after which water

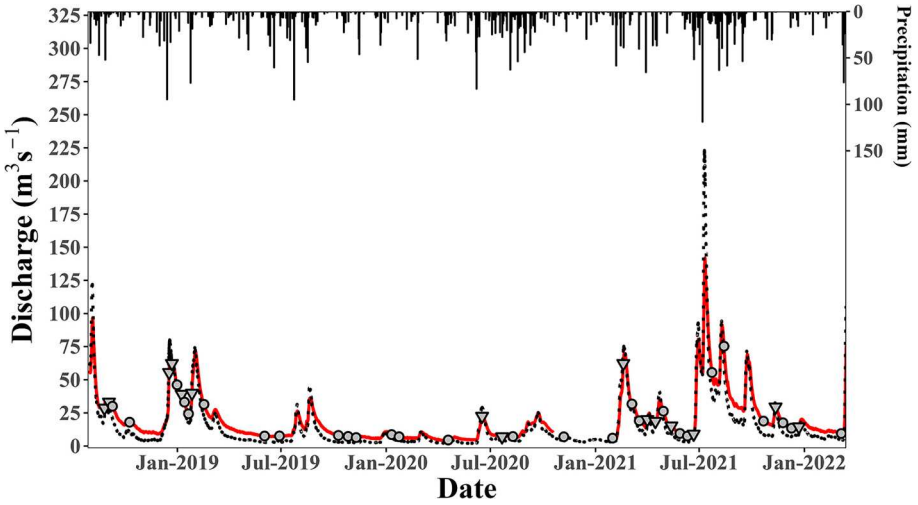

Fig. 2. Hydrographs and daily precipitation for the Sink-Rise system during the 2018–2022 study period. The dotted black line represents river recharge into River Sink (USGS gauging station 02321898). The solid red line represents River Rise discharge (USGS gauging station 02321958). Precipitation data (black bars) were retrieved from the Suwannee River Water Management District database for the gauge located at O'leno State Park (Suwannee River Water Management District, 2024). Paired samplings from River Sink and River Rise where the mixing model indicates dissolution (i.e., positive ΔCa^{2+} values) are marked with grey triangles while grey circles mark samplings where the model indicates precipitation (i.e., negative ΔCa^{2+} values). (For interpretation of the references to colour in this figure legend, the reader is referred to the web version of this article.)

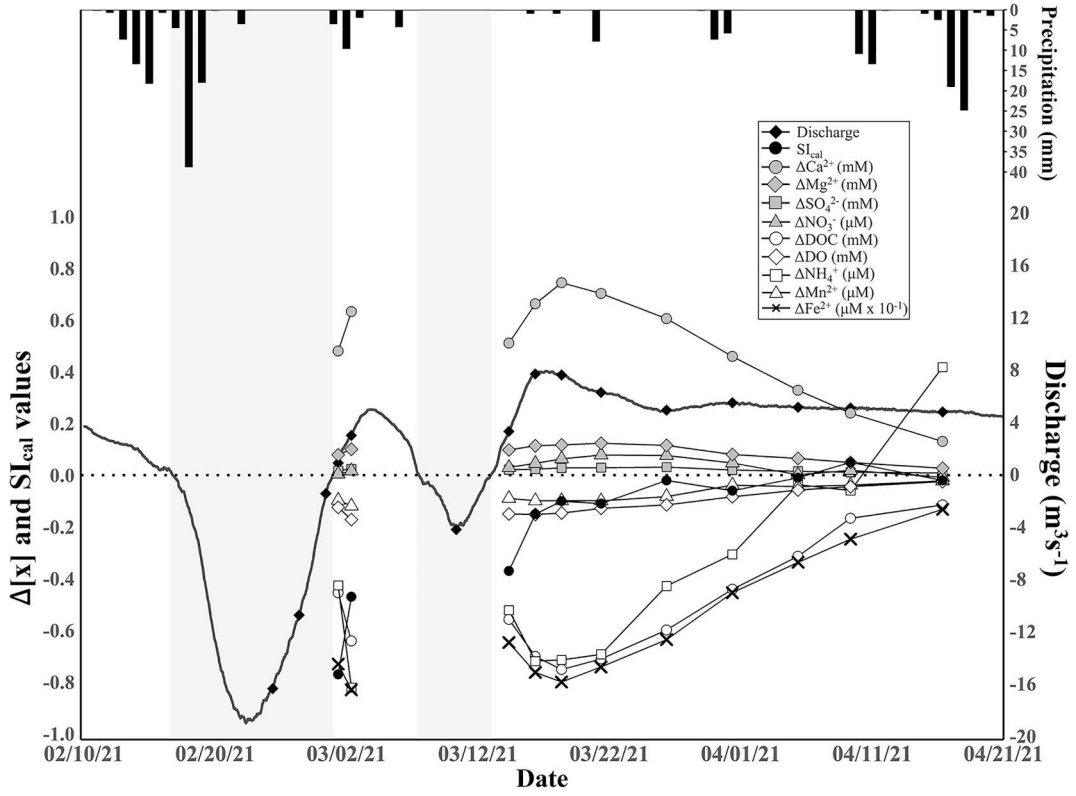

Fig. 3. Hydrograph, daily precipitation, SI_{cal} values, Δ[x] values for solutes during the 2021 spring reversal at Madison Blue Spring. Black diamonds on the hydrograph represent when water samples were collected. Note that units for Δ[x] values are either mM or µM and that ΔFe^{2+} values are multiplied by 10^{-1}. Periods of negative discharge (grey shaded regions) indicate when Withlacoochee River stage exceeded the hydraulic head of groundwater at the spring vent allowing surface water to intrude into the spring system (i.e. recharge phase). The dotted line marks the shift between discharge and surface water intrusion at the spring vent. Data were taken from USGS gauging station 02319302. Precipitation data were retrieved from the Suwannee River Water Management District database for the gauge located at Madison Blue Springs (Suwannee River Water Management District, 2024). (For interpretation of the references to colour in this figure legend, the reader is referred to the web version of this article.)

samples were collected. Water was pumped from monitoring wells using a Proactive Environmental Products 12-Volt Submersible Tornado Pump, installed at a depth of 0.5 m below the water table. The pump was connected to an overflow cup that contained the multiparameter meter electrodes with PVC tubing. Samples were collected after purging at least three well-volumes and the multiparameter meter values

stabilized.

Water was sampled for measurement of ion (Ca^{2+}, Mg^{2+}, Na^{+}, K^{+}, Cl^{-}, SO_4^{2-}, F^{-}, NH_4^{+} NO_3^{-}, Fe, and Mn), dissolved inorganic carbon (DIC), and dissolved organic carbon (DOC) concentrations. Samples were filtered with in-line 0.45 μm GeoTech medium-capacity capsule filters prior to collection. Most ion and dissolved metal samples were collected in two 20 ml HDPE bottles. One bottle was used to measure cation concentrations and was acidified to pH < 2 in the field with trace-metal grade nitric acid. The other bottle was used to measure anion concentrations and had no added preservatives. Instrument detection limits (DL) were determined with sample blanks or from instrument manufacturer specifications. Ion concentrations (except NH_4^{+}) were measured by ion chromatography on Dionex ICS-2100 (anions; DL 1 μM) and ICS-1100 (cations; DL 1 μM) instruments. Samples for NH_4^{+} concentration were collected in 50 ml falcon tubes and frozen until measured by colorimetry on a Seal AA3 AutoAnalyzer (Method G-171-96; DL 0.05 μM). DOC samples were collected in 40 ml amber glass vials combusted at 550 °C before use and were acidified with hydrochloric acid to pH < 2 in the field. DOC was measured on a Shimadzu TOC-VCSN total organic carbon analyzer (DL 10 μM). DIC samples were sequentially filtered with in-line 0.45 μM capsule filters followed by 0.22 μM cellulose filters into 20 ml Qorpac glass vials and sealed with no headspace. DIC concentrations were measured on a UIC 5011 CO_2 coulometer (DL 15 μM) coupled with an AutoMate Preparation Device. All samples were stored on ice in the field and refrigerated at 4 °C or frozen (NH_4^{+} samples) upon return to the lab.

Cation samples collected during the 2021 reversal at Madison Blue Spring were used for analysis of Fe^{2+}(DL 6 nM) and Mn^{2+} (DL 0.2 nM) concentrations on a ThermoFinnigan Element 2 ICP-MS (e.g., Brown et al., 2019). Dissolved trace metal concentrations were corrected with an 18.2 MΩ cm^{-1} water sample blank acidified with the same trace-metal grade nitric acid used in the field and stored in a new 20 ml HDPE bottle.

2.4. Subsurface residence time of river water at the sink-rise system and Madison Blue Spring

Residence times for water flowing through the Sink-Rise system were estimated from an established relationship between River Sink gage height and time for temperature anomalies to travel from River Sink to River Rise (Bailly-Comte et al., 2011; Martin and Dean, 2001; Martin and Dean, 1999). Residence times average 1.8 days and range between <1 and 15 days, with an inverse exponential relationship with discharge. An assumption in these calculations is water flows directly from River Sink to River Rise without exchange between the conduit matrix porosity, which will lengthen the travel times (Martin and Dean, 2001).

The method for estimating subsurface residence time of water recharged during the reversal at Madison Blue Spring is based on a last in-first out accounting of the river water injected during the recharge phase and discharged during recession phase of the reversal as described in Oberhelman et al. (2024). Briefly, subsurface residence times estimated by this method represent the lengths of time between the end of the recharge phase and sample collection plus the time required for the same volume of river water discharged during that period to flow into the spring during the recharge phase of the reversal. These volumes of water are derived from discharge measurements reported for the USGS Gage 02321958 located in the spring run.

2.5. Evaluation of redox and dissolution reactions

End-member mixing models were used to separate solute concentrations linked to mixing of source water from changes in concentrations caused by redox and dissolution reactions at the Sink-Rise system and Madison Blue Spring. Proportions of three sources of water to River Rise were determined using a model developed by Moore et al. (2009) that relies on SO_4^{2-} and Mg^{2+} concentrations. The sources include (1) surface water recharging the aquifer at River Sink, (2) shallow groundwater represented by water collected at Well 4, and (3) deep upwelling mineralized groundwater represented by water collected at Well 2 (Fig. 1B). While SO_4^{2-} and Mg^{2+} may be influenced by redox conditions and various mineral dissolution reactions, they are conservative at the Sink-Rise system based on strong linear correlations of their concentrations between the three source waters (Moore et al., 2009). Additionally, unlike Cl^{-} and Na^{+}, which also behave conservatively, SO_4^{2-} and Mg^{2+} concentrations differ by orders of magnitude among the three source waters, providing robust estimates of surface water and shallow groundwater contributions to River Rise (Oberhelman et al., 2023b). Fractions of river water, shallow groundwater, and deep groundwater were calculated with the following system of equations:

$$1 = X_s + X_{W2} + X_{W4} \tag{6}$$

$$Mg_R = X_S Mg_S + X_{W2} Mg_{W2} + X_{W4} Mg_{W4} \tag{7}$$

$$SO_{4R} = X_s SO_{4S} + X_{W2} SO_{4W2} + X_{W4} SO_{4W4} \tag{8}$$

where the subscripts denote River Sink (S), Well 4 (W4), Well 2 (W2), and River Rise (R). X denotes the fraction of each endmember. Mg^{2+} and SO_4^{2-} denote the average concentrations of Mg^{2+} and SO_4^{2-} from samples at Well 4 and Well 2, while for River Sink and River Rise they denote Mg^{2+} and SO_4^{2-} concentrations for pairs of samples collected on the same day at River Sink and River Rise.

At Madison Blue Spring binary mixing is assumed between spring water and Withlacoochee River water. Proportions of the two sources are determined based on average Cl^{-} concentrations in groundwater discharging at the spring vent during baseflow (0.17 mM) and intruding river water (0.21 mM) during a spring reversal (Brown et al., 2014). Local diffuse recharge to the aquifer through the land surface is assumed to be insignificant relative to the volumes of groundwater and river water that mix within the ~30 m deep conduits during reversals. Fractions of river water and groundwater were calculated by:

$$1 = X_{gw} + X_{rw} \tag{9}$$

$$Cl_{obs} = X_{gw} Cl_{gw} + X_{rw} Cl_{rw} \tag{10}$$

where water discharged following the reversal includes variable fractions of groundwater (X_{gw}) and intruded river water (X_{rw}) at the spring vent. Cl_{obs} is the concentration of Cl^{-} measured in samples during the recession phase of the reversal, Cl_{gw} is the average Cl^{-} concentration in spring discharge at baseflow, and Cl_{rw} is the average Cl^{-} concentration of intruding river water during the recharge phase of the reversal.

Changes in the concentration of solutes, including major ions, DOC, metals, DO caused by redox and dissolution reactions were assessed by:

$$\Delta[x] = [x]_{observed} - [x]_{mix} \tag{11}$$

where [x] represents the solute of interest and Δ[x] is the difference between the observed concentration ($[x]_{observed}$) and the concentration predicted by mixing of source waters ($[x]_{mix}$) based on Eqs. (6)–(10). Positive Δ[x] values represent a net gain of solutes from reactions and negative Δ[x] values represent a net loss of solute from reactions. A Δ[x] value of zero indicates conservative behavior.

Dissolution and precipitation of limestone are represented as forward or reverse reaction:

$$CaCO_3 + H^{+} \leftrightarrow Ca^{2+} + HCO_3^{-} \tag{12}$$

where H^{+} represents a generic acid, most likely carbonic, sulfuric, or nitric. The mass of limestone dissolved or precipitated ($\Delta CaCO_3$, kg) was estimated for individual samples from the Sink-Rise system by:

$$\Delta CaCO_3 = \Delta Ca^{2+} \times R \times Q \times M \tag{13}$$

where ΔCa^{2+} is the Δ[x] value for Ca^{2+} (mol l^{-1}), R is the subsurface residence time (s), Q is the discharge (l s^{-1}) at River Rise (USGS Gage 02321958; Fig. 2) at the time of sampling, and M is the molar mass of calcite (0.10009 kg mol^{-1}).

The mass of calcite dissolved or precipitated during the sampled reversal at Madison Blue Spring was estimated by multiplying discharge volumes by ΔCa^{2+} values of samples, using the following algorithm because sampling and discharge measurements occurred at different frequencies. The volume of discharge (Vm, l) centered on the time for each sample was calculated from:

$$Vm = Qm \times 900 \quad (14)$$

where Qm (l s^{-1}) is the sum of reported discharge values centered on the sampling time and bounded by times midway between the previous and subsequent samples (Fig. S1). The value 900 converts the sum discharge values to flow volume under the assumption of constant discharge over each 15-min interval. For the initial sample after the recharge phase of the reversal, Qm is based on sum of discharge from the end of the recharge phase (identified as positive discharge, Fig. 3 and S1) to midway between the time for the first and the second samples. At the end of the record, Qm is based on the midpoint between the penultimate and ultimate sample through the end of the recession phase of the reversal which we define as when another reversal begins or when the discharging water is <5% river water. Because our final sample contains ~11% river water (Fig. 3), we identify the end of the recession phase by extrapolating a regression of the natural log of the river water fraction through time (Eqs. (9) and (10)) in the last five samples to a value of 5% river water (Oberhelman et al., 2023b). The mass of calcite dissolution or precipitation was based on each sample's composition during the recession phase and calculated by:

$$\Delta CaCO_3 = Vm \times \Delta Ca^{2+} \times M \quad (15)$$

The sum of $\Delta CaCO_3$ values of all samples collected during the recession period equals the total dissolution or precipitation for the reversal.

Calcite can contain variable amounts of Mg^{2+} substituting for Ca^{2+} in the crystal lattice and limestones may contain additional Mg^{2+} in the form of dolomite ($CaMg(CO_3)_2$) resulting in an underestimate of dissolution if calculations are based solely on ΔCa^{2+} values. We thus include ΔMg^{2+} values in the total dissolution, which converts the mass balance (Eq. (13)) to:

$$(Mg_x, Ca_{1-x})CO_3 + H^+ \leftrightarrow xMg^{2+} + (1-x)Ca^{2+} + HCO_3^- \quad (16)$$

where x is the mole fraction of $MgCO_3$ in the dissolving rock with x = ~0.5 for dolomite. Total carbonate mineral dissolution is estimated as the sum of calcite dissolution and $MgCO_3$ dissolution, which is calculated with Eqs. (14) and (15) by substituting ΔMg^{2+} values for ΔCa^{2+} values and instead using the molar mass of $MgCO_3$ (0.08431 kg mol^{-1}). This assessment was only made at Madison Blue Spring because Mg^{2+} concentrations constrain the mixing models at the Sink-Rise system.

We estimate the amount of acid that could be produced by oxidation of the following common species (1) DOM, (2) pyrite, (3) NH^{4+}, (4) iron (II), and (5) manganese(II) (Table 1, Eqs. (1)–(5)) using reaction stoichiometry and by assuming each reaction is responsible for the entire Δ[x] value of measured solutes, excluding DO, involved in that reaction. Oxidation of DOM is represented by ΔDOC values assuming a Redfield ratio (C:N:P = 106:16:1). NO_3^- is also produced when DOM is oxidized (e.g. Gao et al., 2023; Eq. (1)) but the amount of NO_3^- produced by assuming ΔDOC values represent DOM is not significant compared to observed ΔNO_3^- values and thus we do not consider it further. Pyrite oxidation is represented by ΔSO_4^{2-} values. Oxidation of NH_4^+ is represented using both ΔNH_4^+ and ΔNO_3^- values. Iron(II) and manganese(II) oxidation are represented using ΔFe^{2+} and ΔMn^{2+} values, respectively. Acid produced by reactions 1–5 (Table 1) is represented as H^+ or CO_2, which hydrates to form carbonic acid (Eq. (17)) that dissociates to produce H^+.

$$CO_2 + H_2O \leftrightarrow H_2CO_3 \leftrightarrow H^+ + HCO_3^- \quad (17)$$

The mass of dissolution is estimated for each redox reaction assuming all produced acid dissolved carbonate minerals (e.g., Eq. (12)) and is referred to herein as the dissolution potential. The dissolution potential at Madison Blue Spring is not fractionated between $CaCO_3$ and $MgCO_3$ using the observed x value (e.g., Eq. (16); equivalent to $\Delta Mg^{2+}/(\Delta Ca^{2+} + \Delta Mg^{2+})$) because the difference in the total mass of rock dissolved (e.g., Eq. (15)) is lower than the uncertainty in estimates of dissolution potential. The limitation of dissolution potential for the redox reactions in Table 1 may result from availability of DO. The amount of DO consumption necessary for the full dissolution potential of each redox reaction was estimated using reaction stoichiometry and is referred to herein as the required DO consumption. The amount of DO consumption that occurred based on ΔDO values is termed the observed DO consumption.

The rate of limestone dissolution (μM hr^{-1}) was calculated assuming calcite dissolution at both the Sink-Rise system and Madison Blue Spring and the residence time, Rt (hr) of the water in the subsurface when dissolution reactions occurred:

$$Rate = \Delta Ca^{2+}/Rt \quad (18)$$

The dissolution rate considering Mg-calcite is also calculated at Madison Blue Spring:

$$Rate = \left(\Delta Ca^{2+} + \Delta Mg^{2+}\right)/Rt \quad (19)$$

Dissolution is kept in concentration units to normalize for different fractions of river water between samples.

2.6. Calcite saturation indices and geochemical modeling

We use PHREEQC version 3.7.3 (Parkhurst and Appelo, 2013) with the LLNL database to calculate calcite saturation indices (SI_{cal}) and estimate the amount of dissolution that could result from the initial undersaturation of recharged surface water. We estimate dissolution from the initial undersaturation of recharged surface water by first deriving the chemical composition of water that would discharge if only conservative mixing of source waters occurred (i.e. no reactions in the subsurface) using the mixing fractions estimated for source waters in each sample (Eqs. (6)–(10)). We then simulate calcite dissolution by reacting the derived water composition in PHREEQC until the SI_{cal} value equals the SI_{cal} value of that sample based on measured solute concentrations. The $QC_{diss.}$ value is calculated as the difference in the Ca^{2+} concentration before and after simulation of calcite dissolution converted to kg of calcite following Eqs. (13)–(15). $QC_{diss.}$ thus represents the amount of calcite that could be dissolved by acid in recharging water, which includes any acidity supplied by the equilibration of the water with atmospheric CO_2, the hydration of CO_2 generated by stream heterotrophy, and the presence of mineral and organic acids.

We define the relative amounts of additional acids needed to support dissolution (A_{acid}) as the difference between dissolution estimated from source water mixing models (i.e., ΔCa^{2+}, Eqs. (13)–(15)) and $QC_{diss.}$:

$$A_{acid} = \Delta Ca^{2+} - QC_{diss.} \quad (20)$$

If A_{acid} is positive, more dissolution occurred than can be explained by initial river water undersaturation and additional acid is needed, in which case, A_{acid} also represents the amount of dissolution caused by acid provided by subsurface redox reactions. The A_{acid} /ΔCa^{2+} ratio represents the fraction of total dissolution derived from these sources. If A_{acid} is negative, injected river water has sufficient acid for the amount of dissolution that was observed based on the ΔCa^{2+} value.

Calculations of $QC_{diss.}$ and SI_{cal} values in PHREEQC use water compositions based on temperature, pH, and DO, DIC, Ca^{2+}, Mg^{2+}, Na^+, K^+,

F^-, Cl^-, SO_4^{2-}, NO_3^-, and NH_4^+ concentrations with charge balance forced with alkalinity. Fe^{2+} and Mn^{2+} concentrations were also included for Madison Blue Spring samples. We consider SI_{cal} values of 0 ± 0.3 to indicate equilibrium based on analytical and thermodynamic data uncertainty (Lu et al., 2022; Moore et al., 2010). Pure calcite dissolution is assumed in PHREEQC modeling.

3. Results

3.1. SI_{cal} and dissolution

The ΔCa^{2+} values at the Sink-Rise system indicate periods of both calcite dissolution ($n = 15$) and precipitation ($n = 28$), with dissolution predominantly occurring during flood events (Fig. 2). The mass of calcite dissolution and precipitation for individual samples ranged from 0.09 × 10^4-9 × 10^4 kg dissolution to 0.04 × 10^4-11 × 10^4 kg precipitation. Across all Sink-Rise system samples, there was 24 × 10^4 kg of dissolution and 115 × 10^4 kg of precipitation. In contrast, only dissolution occurred during the reversal at Madison Blue Spring. A total of 106 × 10^4 kg of rock dissolved during the reversal, of which 92 × 10^4 and 14 × 10^4 kg were calcite and Mg-calcite, respectively.

Median SI_{cal} values across all sample locations ranged from −1.2 to 0.34 (Fig. 4). All well water and reversing spring samples had median SI_{cal} values of 0 ± 0.1 except Otter Spring, which had a value of 0.34 ± 0.21. Median SI_{cal} values at River Sink, Sweetwater Lake, and River Rise were − 1.2, −0.84, and − 0.56, respectively, and show a larger range than other locations. The range of median SI_{cal} values at River Sink during baseflow was −0.31 and during flood events decreased to −1.6. During baseflow, SI_{cal} values indicate water flowing through the Sink-Rise system reaches equilibrium with calcite. At Madison Blue Spring, the median SI_{cal} value during baseflow was −0.08 and during the recharge phase of the reversal decreased to −3.11. SI_{cal} values increased from −0.77 to 0.05 during the recession phase (Fig. 3) and recovered to baseflow values when returning surface water had a residence time of ~730 h.

The A_{acid} values (Eq. (20)) are positive for all samples collected following the reversal at Madison Blue Spring (Fig. 5A). At the sink Rise system, A_{acid} values are mostly negative and increase with residence times, becoming positive in two cases (Table 2) when recharged water had residence times between 20 and 60 h. The increase of A_{acid} values extend to a maximum of 7.0 × 10^4 kg at a residence time of ~720 h with values decreasing to near zero at longer residence times. For samples with positive $A_{acid.}$ values, the $A_{acid}/\Delta Ca^{2+}$ ratio remains fairly constant with a median value of 0.53 ± 0.07 (Fig. 5B).

Assuming pure calcite, the calculated $QC_{diss.}$ indicate the initial undersaturation of recharged surface waters during the reversal at Madison Blue Spring could dissolve 43 × 10^4 kg of calcite, or ~ 47% of the total observed dissolution (Fig. 6). The calculated $QC_{diss.}$ values also indicate the initial undersaturation of surface waters could dissolve 2.1 × 10^4 and 1.2 × 10^4 kg of calcite for the two samples with positive A_{acid} values at the Sink-Rise system (Fig. 5A; Table 2). These masses of calcite represent 49% and 55% of the total observed dissolution in those samples, respectively.

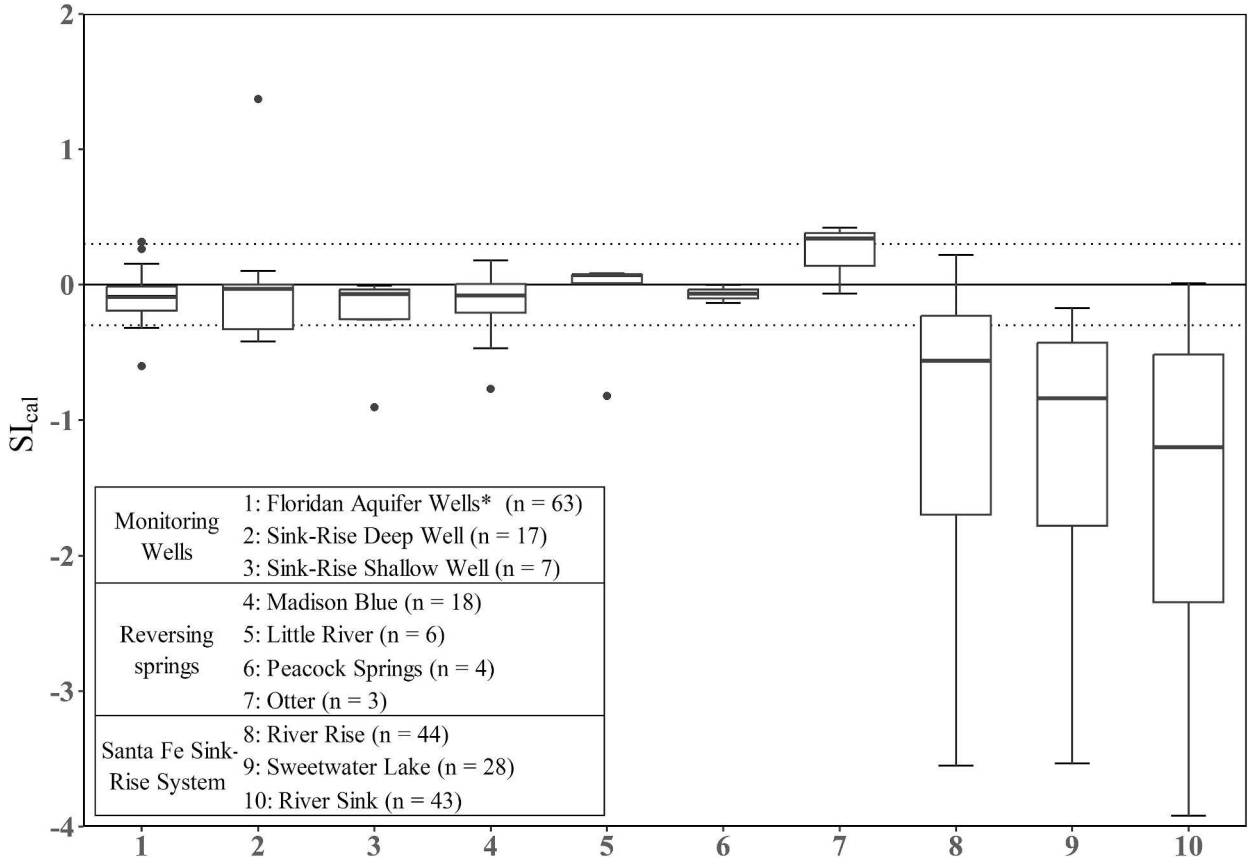

Fig. 4. Boxplots of saturation indices with respect to calcite (SI_{cal}) at springs and monitoring wells. The solid line represents an SI_{cal} of zero while the dashed lines represent ±0.3, which is the range we consider here to indicate a sample is at equilibrium with calcite. Samples from the recharge phase of the reversal at Madison Blue Spring were excluded from this plot as they represent the SI_{cal} of river water not spring discharge. The median SI_{cal} of these four excluded samples is reported in the text. Boxplots follow the standard Tukey convention. *Includes data from McMahon et al. (2017). (For interpretation of the references to colour in this figure legend, the reader is referred to the web version of this article.)

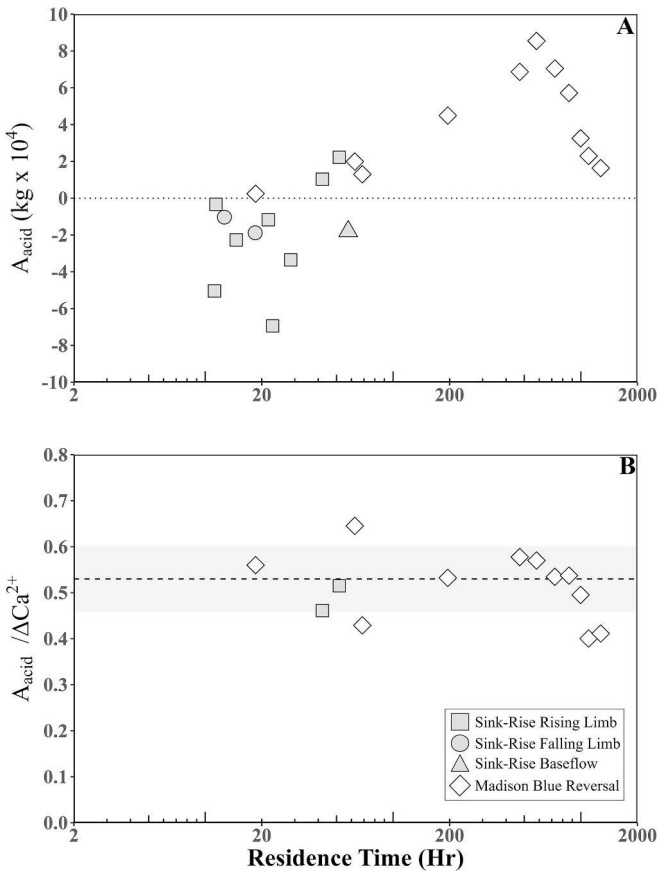

Fig. 5. (**A**) A_{acid} (Eq. (20)) versus subsurface residence time at the Sink-Rise system and Madison Blue Spring. The dotted line on A marks where A_{acid} = 0 (i.e., $\Delta Ca^{2+} = QC_{diss.}$). Values that fall below the dotted line identify samples where PHREEQC modeling indicates the amount of dissolution based on ΔCa^{2+} values could be supported by undersaturation of the recharged waters and no additional acids are required for the observed dissolution. Values that fall above the dotted line identify samples where PHREEQC modeling indicates acid in addition to undersaturation of recharging river water is required generate the amount of dissolution based on ΔCa^{2+} values. (**B**) A_{acid} /ΔCa^{2+} versus subsurface residence time at the Sink-Rise system and Madison Blue Spring for samples where A_{acid} is positive. A_{acid} /ΔCa^{2+} indicates the fraction of dissolution derived from additional acids and has a median value of 0.53 ± 0.07 represented by the dashed line and grey shaded region. (For interpretation of the references to colour in this figure legend, the reader is referred to the web version of this article.)

Table 2
Dissolution for Sink-Rise system samples with positive A_{acid} values.

Date	ΔCa^{2+} (10^4 kg)	$QC_{diss.}$ (10^4 kg)	A_{acid} (10^4 kg)
21-06-2021	4.3	2.1	2.2
22-12-2021	2.2	1.2	1.0

3.2. Reactive changes to solute concentrations

Following the reversal at Madison Blue Spring, Δ[x] values indicate a reactive loss of DO, DOC, NH_4^+, Mn^{2+}, and Fe^{2+} and gain of Ca^{2+}, Mg^{2+}, SO_4^{2-}, and NO_3^- (Fig. 3). For the two Sink-Rise system samples with positive A_{acid} values (Fig. 5), Δ[x] values indicate a reactive loss of DO, DOC, and NH_4^+ and gain of Ca^{2+} and NO_3^- (Table 3). The use of Mg^{2+} and SO_4^{2-} concentrations to evaluate mixing and lack of measurements of Mn^{2+} and Fe^{2+} concentrations prevent estimates of their reactive loss or gain at the Sink-Rise system.

Anoxia was not observed at the Sink-Rise system or Madison Blue Spring (Oberhelman et al., 2023a). At Madison Blue Spring, the lowest DO concentration was 1.0 mg/l (~10% saturation) in the sample collected ~80 h after the end of the reversal following a subsurface residence time of ~200 h. At River Rise, the lowest DO concentration was 0.7 mg/l (~8% saturation) and occurred during baseflow when discharge was 7.2 m^3/s, including ~15% surface water (Eqs. (6)–(8)) with a subsurface residence time of ~66 h.

3.3. Potential dissolution from redox generated acids and required DO consumption

At Madison Blue Spring, the dissolution potential derived from DOM oxidation based on ΔDOC values is 105 × 10^4 kg of calcite (Fig. 6). This value is greater than the difference between dissolution based on ΔCa^{2+} + ΔMg^{2+} values (Eqs. (13)–(15)) and $QC_{diss.}$, which is 63 × 10^4 kg calcite. The dissolution potential of non-carbonic acids, derived from nitrification and oxidation of pyrite, iron(II), and manganese(II), is ~24 × 10^4 kg calcite, which is ~1/4 of the dissolution potential of DOM oxidation. For the two Sink-Rise system samples with positive A_{acid} values, the dissolution potential from DOM oxidation based on ΔDOC values is sufficient to dissolve 9.2 × 10^4-25 × 10^4 kg of calcite (Table 3), which is enough to make up the difference between dissolution based on ΔCa^{2+} and $QC_{diss.}$ for both samples (Table 2). The dissolution potential of nitrification provides <1 × 10^4 kg of calcite dissolution for the two Sink-Rise samples (Table 3).

The observed DO consumption was 88 μM at Madison Blue Spring over the entire sampled reversal and is ~8 times smaller than the total required DO consumption of 660 μM for the reactions listed in Table 1 to go to completion based on the Δ[X] values (Fig. 7). The deficit in available DO is especially acute for DOM oxidation, which requires ~6 times greater DO consumption than was observed, although the required DO consumption for each of the other redox reactions (Eqs. (2)–(5)) is less than observed. Similarly at the Sink-Rise system, the observed DO consumption for the two samples with positive A_{acid} values were smaller than required DO consumption for DOM oxidation but greater than the required DO consumption for nitrification (Table 3).

3.4. Dissolution rates

At Madison Blue Spring, dissolution rates for pure calcite range from 0.1 to 26 μM calcite hr^{-1} (Eq. (18); Fig. 8). Dissolution rates increased by ~17%, assuming ΔMg^{2+} also represents carbonate dissolution and ranged from 0.1 to 30 μM calcite hr^{-1} (Eq. (19)). Dissolution rates at the Sink-Rise system ranged from 0.3 to 15 μM calcite hr^{-1} (Eq. (18)). Maximum dissolution rates at both Madison Blue Spring and the Sink-Rise system occur with subsurface residence times between 20 and 40 h with minimum values <0.2 μM calcite hr^{-1} as subsurface residence times decrease to ~10 h and increase to ~1500 h.

4. Discussion

The following discussion explores how exchange of surface water and groundwater, variable residence times of recharged water in the subsurface, and production of various acids resulting from redox reactions contribute to dissolution in carbonate aquifers. We use the A_{acid}/ΔCa^{2+} to compare dissolution from undersaturation of recharging surface water to that from acid generated by subsurface redox reactions (Table 1). We separate acids derived from various redox reactions through mass balance relationships of electron donor and acceptor concentrations. The mass balance calculations allow estimates of dissolution kinetics, how reactions rates may impact dissolution, and demonstrate maximum dissolution rates occur at specific subsurface residence times. Although the study location is north-central Florida, USA, findings and developed analytical methods may be applicable to general understanding of dissolution and mobilization of carbon in the

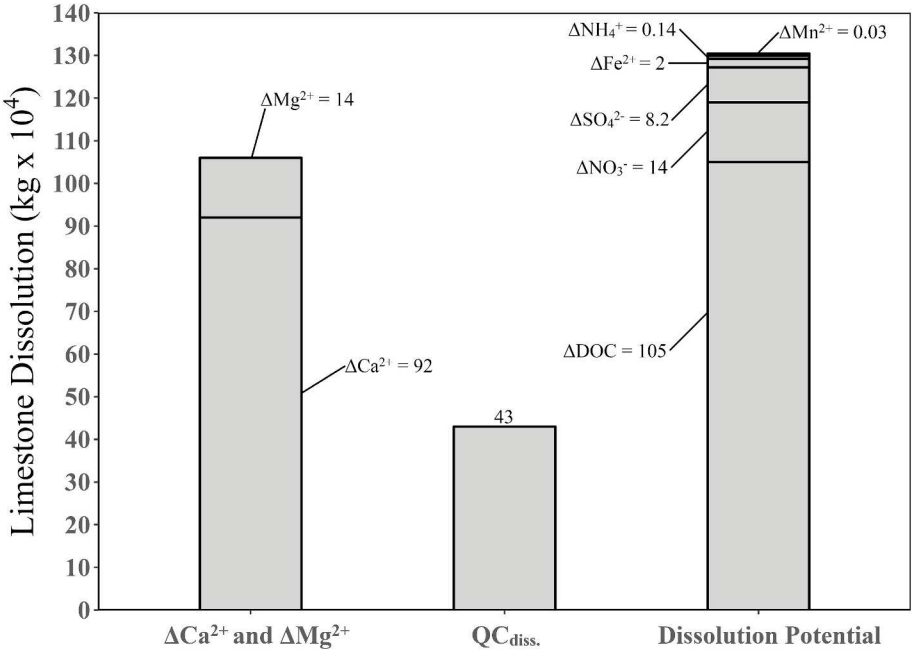

Fig. 6. Bar plot showing the amounts of dissolution based on ΔCa^{2+} and ΔMg^{2+} values, the amount of dissolution attributed to the initial undersaturation of surface water based on PHREEQC modeling (QCdiss.), and the potential dissolution from acid generated during various redox reactions (Table 1) during the sampled reversal at Madison Blue Spring. The sum of potential dissolution from production of various acids by redox reactions exceeds the difference between dissolution based on ΔCa^{2+} values and QC_{diss}. (For interpretation of the references to colour in this figure legend, the reader is referred to the web version of this article.)

Table 3
Δ[x] values, dissolution potential, and required DO consumption for Sink-Rise system samples with positive A_{acid} values. Note that ΔDO represents the observed DO consumption.

Date	Ca^{2+}	DO	DOC	NH_4^+	NO_3^-
			(Eq. (1))	(Eq. (3))	(Eq. (3))
Δ[x] values (mM)					
21-06-2021	0.26	−0.05	−1.28	−0.003	0.02
22-12-2021	0.10	−0.09	−0.36	−0.002	0.02
Dissolution Potenital (10^4 kg):					
21-06-2021	–	–	25	0.1	0.5
22-12-2021	–	–	9.2	0.1	0.9
Required DO consumption (μM):					
21-06-2021	–	–	1700	3.5	15.9
22-12-2021	–	–	470	2.2	20.8

carbonate critical zone.

4.1. Dissolution and subsurface residence time

At long residence times (> ~60 h), the amount of carbonate dissolution estimated from ΔCa^{2+} values cannot result from the initial undersaturation of the recharged water ($QC_{diss.}$) (Fig. 5A). At residence times between 10 and 60 h, the undersaturation state of the recharged water is sufficient to cause all of the dissolution indicated by ΔCa^{2+} values for most samples with negative A_{acid} values. Exceptions occur in three additional samples with residence time of ~20 to 60 h, where additional sources of acid are required for dissolution indicated by ΔCa^{2+} values.

Acid produced by reactions 1–5 (Table 1) is sufficient to supply the needed additional acid (Tables 2, 3; Fig. 6) and these acids would immediately begin to contribute to dissolution once produced, even for samples with negative A_{acid} values (Fig. 5A). That dissolution begins immediately after acid production is supported by low variability of the

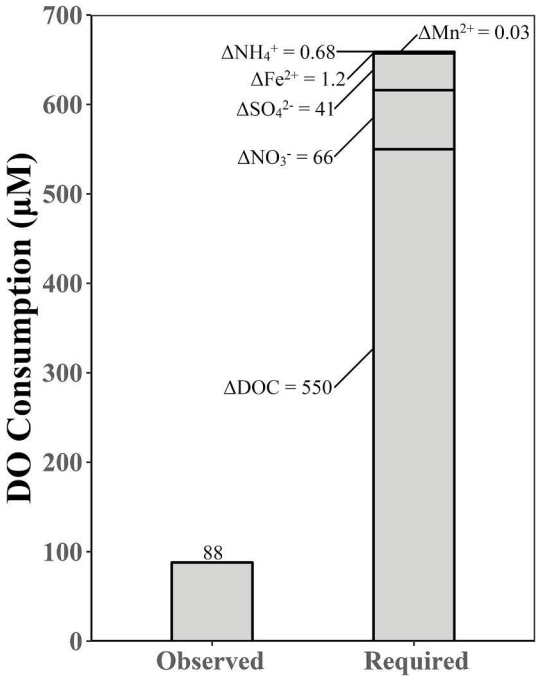

Fig. 7. Bar plot showing the observed DO consumption and the DO consumption required to actualize the dissolution potential based values of redox sensitive solutes (Fig. 6) at Madison Blue Spring based on redox reaction stoichiometry (Table 1). Observed DO consumption is insufficient to actualize the dissolution potential based values of redox sensitive solutes. (For interpretation of the references to colour in this figure legend, the reader is referred to the web version of this article.)

A_{acid} /ΔCa^{2+} values (0.53 ± 0.07; Fig. 5B) in samples with positive A_{acid} values. Acid concentrations, from both recharged undersaturated surface water and through production in the subsurface via reactions 1–5

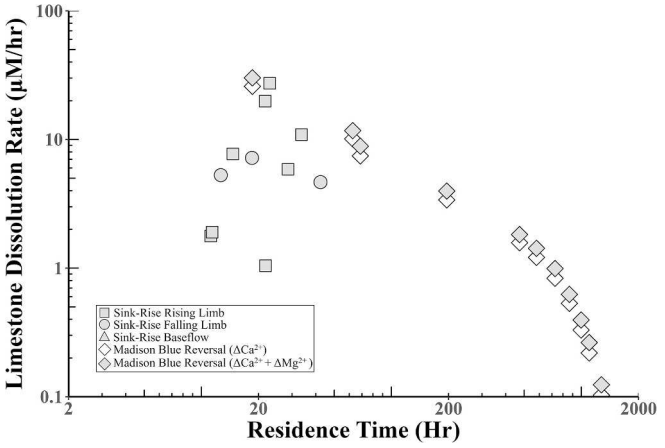

Fig. 8. Plots showing the dissolution rate of limestone versus subsurface residence time at the Sink-Rise system and Madison Blue Spring. The rate for pure calcite dissolution (ΔCa^{2+}) and Mg-calcite ($\Delta Ca^{2+} + \Delta Mg^{2+}$) dissolution are displayed for Madison Blue Spring. (For interpretation of the references to colour in this figure legend, the reader is referred to the web version of this article.)

(Table 1), exceed those required for the observed dissolution (ΔCa^{2+} values), indicating the rate of acid production from redox reactions is faster than acid consumption from calcite dissolution, and thus the kinetics of acid production exceed those of calcite dissolution.

Dissolution by acids produced in the subsurface (Eqs. (1)–(5)) may represent a source of CO_2 to the atmosphere. Remineralization of DOM and dissolution by produced acids increases the pCO_2 and DIC concentration of the water, and CO_2 will evade to the atmosphere where pCO_2 is greater than atmospheric equilibrium. However, loss of atmospheric CO_2 by carbonic acid dissolution of carbonate minerals is net neutral for atmospheric CO_2 over geologic time because the consumed CO_2 returns to the atmosphere during carbonate mineral precipitation (Eqs. (12), (17); Berner et al., 1983):

$$Ca^{2+} + 2HCO_3^- \rightarrow CaCO_{3(s)} + H_2O + CO_{2(g)} \quad (21)$$

In contrast, dissolution by non-carbonic acids, such as sulfuric and nitric acids, produces DIC without the balancing consumption of atmospheric CO_2 making any subsequent carbonate mineral precipitation a net source of atmospheric CO_2 (Martin, 2017; Liu et al., 2010, 2011; Martin et al., 2013).

We use the stoichiometry of carbonate mineral precipitation (Eq. (21); the reverse of dissolution) to estimate the potential mass of CO_2 that could be released by subsurface reactions via the remineralization of organic carbon (Eq. (1)) and dissolution by non-carbonic acids (Eqs. (2)–(5)) at the Sink-Rise system and during the Madison Blue Spring reversal. We multiply the median fraction of dissolution from redox reactions (0.53 ± 0.07) by the total calcite dissolution observed at both sites during this study ($92 \times 10^4 + 24 \times 10^4 = 116 \times 10^4$ kg $CaCO_3$). This calculation indicates that between 20 and 30 $\times 10^4$ kg of CO_2 is mobilized by the remineralization of organic carbon and dissolution by non-carbonic acids. However, not all of the produced CO_2 may evade to the atmosphere if some is fixed as organic carbon and buried in sediments (e.g., the biological pump; Liu and Dreybrodt, 2015; Liu et al., 2010). In addition, where recharged surface water has sufficient undersaturation for all observed dissolution (i.e., negative A_{acid} values, Fig. 5A), mobilized CO_2 could be less, but we lack data needed to evaluate this difference.

4.2. ΔDOC values and possible redox reactions contributing additional acid

Only one sample with positive A_{acid} values had sufficient observed DO consumption to produce the amount of acid required for dissolution indicated by ΔCa^{2+} values (Table 3, sample collected on 12/22/2021). The observed DO consumption (Fig. 7; Table 3) would need to be 6, 34, and 5 times greater to produce the Δ[x] values linked to acid production from reactions 1, 2, and 3 (Table 1) during the Madison Blue Spring reversal and for the two Sink-Rise system samples with positive A_{acid} values, respectively. Consequently, anaerobic redox reactions would also have to produce acids contributing to carbonate dissolution. However, because all samples evaluated here contained some DO, the dissolution potential of anerobic redox reactions was not quantified.

Although anerobic redox reactions appear to contribute to dissolution by production of acid, positive Δ[x] values for NO_3^- and SO_4^{2-} (Fig. 3 and Table 3) suggest two common anaerobic reactions, denitrification and sulfate reduction (Eq. (22) and (23) in Table 4), do not occur. Additional anaerobic acid-producing reactions include fermentation and humification reactions and the oxidation of organic carbon with humic substances (Eqs. (25)–(27) in Table 4), which would also contribute to observed DOC losses. Another anerobic carbon reaction that may contribute acid is methanogenesis (Eq. (24) in Table 4). Methanogenesis, which can produce CO_2 (e.g., Ferry, 2011; Mattson and Likens, 1993), has been observed previously at Madison Blue Spring during the recession phase based on CH_4 concentrations changes and $\delta^{13}C$-CH_4 values (Oberhelman et al., 2023b). Conditions must be more reducing for methanogenesis than for denitrification and sulfate reduction, indicating subsurface redox conditions are heterogenous, likely both spatially across microenvironments and in time during surface water-groundwater exchange periods.

Heterogeneous conditions during reversals would result from flow paths through and temporary storage in various types of pore spaces, including factures, matrix porosity, and conduits. Heterogeneity of flow paths and temporary storage will mix water from microenvironments with diverse redox conditions and overprint the signal of one or more redox reaction. For example, the insufficient availability of DO for aerobic redox reactions and indications of methanogenesis suggest denitrification and sulfate reduction occur regardless of the positive ΔNO_3^- and ΔSO_4^{2-} values (Fig. 3 and Table 3). Heterogeneous distribution of redox conditions highlights that only bulk chemical changes are sampled as recharged river water returns to the surface.

Losses of DO insufficient to explain losses of DOC solely by remineralization (Eq. (1)) suggest other process may also cause DOC loss. These processes could include adsorption onto carbonate surfaces or to the iron oxides that are common in the Floridan aquifer (Brown et al., 2019; Brigmon et al., 1994; Martin, 1990). Iron oxides represent the most plausible surface for significant DOC adsorption because adsorption on UFA carbonate minerals is small (0.67 mmol DOC kg^{-1} rock) and reversible (Jin and Zimmerman, 2010). In contrast, iron oxides have high adsorption capacity (Lalonde et al., 2012; Kaiser and Guggenberger, 2003), high strength of adsorption (Gu et al., 1994), and new Fe, Mn-oxides form during surface water-groundwater interactions (Brown et al., 2019). Unlike adsorption on carbonate surfaces, however, the amount of DOC adsorbed on Fe,Mn-oxides and their abundance in the UFA are unknown. The lack of this information prevents a quantitative assessment of the magnitude of DOC loss to iron oxide adsorption.

4.3. Dissolution rates and precipitation

Dissolution rates reach a maximum when recharged surface water has an intermediate subsurface residence time of ~60 h (Fig. 8). This maximum represents the time for the greatest interaction of undersaturated water with the aquifer rock as the system approaches equilibrium with respect to calcite (Fig. 3), thereby decreasing dissolution rates (Buhmann and Dreybrodt, 1985). In contrast, at short residence times, particularly in flow-through systems like the Sink-Rise system, large void volumes limit the amount of contact between undersaturated recharged water and aquifer rocks, thereby limiting the amount of dissolution regardless of the initial undersaturation of flood water or the

Table 4
Anerobic redox reactions that may generate acidity based on reaction stoichiometry.

Eq. #	Reaction Name	Chemical Reaction
Eq. (22)	Denitrification[1]	$(CH_2O)_{106}(NH_3)_{16}H_3PO_4 + 84.8HNO_3 \rightarrow 106CO_2 + 148.8H_2O + 16NH_3 + H_3PO_4^{2-} + 42.4\ N_2$
Eq. (23)	Sulfate Reduction[1]	$(CH_2O)_{106}(NH_3)_{16}H_3PO_4 + 53SO_4^{2-} \rightarrow 106CO_2 + 106H_2O + 16NH_3 + H_3PO_4 + 53S^-$
Eq. (24)	Methanogenesis[1]	$(CH_2O)_{106}(NH_3)_{16}H_3PO_4 \rightarrow 53CO_2 + 16NH_3 + H_3PO_4 + 53CH_4$
Eq. (25)	Fermentation[1]	$(CH_2O)_{106}(NH_3)_{16}H_3PO_4 \rightarrow 35.3CO_2 + 16NH_3 + H_3PO_4 + 35.3C_2H_5OH$
Eq. (26)	Humification[1]	$(CH_2O)_{106}(NH_3)_{16}H_3PO_4 \rightarrow 35.3CO_2 + (C_2H_5OH)_{35.3}(NH_3)_{16}H_3PO_4$
Eq. (27)	Humic DOM Oxidation[2]	$C_6H_{12}O_6 + 12AQDS^* + 12H_2O \rightarrow 6HCO_3^- + 12AH_2QDS^{**} + 6H^+$

[1] Mattson and Likens (1993).
[2] Wang et al. (2017).
[*] anthraquinone-2,6-disulfonic acid (laboratory analogue for humic substances).
[**] anthrahydroquinone-2,6-disulfonic acid (reduced form of AQDS).

acid produced in situ by redox reactions. These observations indicate that residence time of the recharged water in the subsurface is more important to the magnitude of dissolution than the volume of recharged surface water or its degree of undersaturation (e.g., Kipper, 2019).

Residence times are likely variable for water recharged during high flow events at the Sink-Rise system. Longer residence times will occur for water flowing from the conduit to matrix porosity than water flowing through the conduits (Fig. 2; Martin et al., 2006; Bailly-Comte et al., 2010). The water retained in matrix porosity will have greater interaction with matrix rocks, both because of longer reaction times and because of the greater surface area of the small pore spaces. This dissolution within the matrix porosity suggests that the residence time required for maximum dissolution could be greater than our estimate of ~60 h (Fig. 8), which would be an average value for the entire system.

In addition to dissolution, calcite precipitation is indicated by losses of Ca^{2+} at the Sink-Rise system and correlations between net gains of DOC and losses of DIC (Oberhelman et al., 2024). Calcite precipitation has been observed in surface water of Florida spring runs because of minor changes in saturation state although authigenic calcite deposits do not form (de Montety et al., 2011). In the subsurface, during baseflow, shifts in equilibrium may cause precipitation because less surface water is captured at River Sink, which also tends to be more saturated with respect to calcite at baseflow, and groundwater that is saturated with respect to calcite makes up a greater proportion of water in the system (Fig. 4). Shifts in equilibrium would result from chemoautotrophic consumption of DIC, which would lower pCO_2 driving Eq. (12) in reverse (Oberhelman et al., 2024). Alternatively, shifts in equilibrium from decreased pCO_2 would result from a drop in pressure due to increased flow velocity as groundwater enters the conduit system from the surrounding aquifer matrix, which induces gas bubble formation (e.g., Agnew and Halihan, 2018). Although a majority of our samples suggest the occurrence of calcite precipitation (Fig. 2), most samples were collected when stream discharge was below the average of 14.3 m^3s^{-1} (24 of 43 samples) at River Sink, while dissolution dominates over precipitation during high flow events (Moore et al., 2010; Screaton et al., 2004). These differences indicate our sampling was skewed toward periods of net precipitation.

4.4. Dissolution and surface water-groundwater interactions

Our data suggest that without recharging surface water, existing spring conduit systems in the UFA would undergo little further dissolution. Spring baseflow and well waters, both of which represent groundwater compositions, are at equilibrium or oversaturated with respect to calcite (Fig. 4; Martin and Gordon, 2000; Gulley et al., 2013a). In contrast, median SI_{cal} values indicate continuous calcite undersaturation for water in the Sink-Rise system, although calite saturation is approached during baseflow and undersaturation diminishes down the flow path. Calcite undersaturation also characterizes recharging surface water during reversals at Madison Blue Spring. Undersaturation at both locations is enhanced by acid produced during redox reactions following recharge and control the evolution of conduit systems in the Floridan aquifer (e.g., Gulley et al., 2011).

Calcite undersaturation may also result from mixing of two water sources with distinct compositions because solute concentrations (Ca^{2+} and CO_3^{2-}) of the mixture have linear relationships while solute activity and calcite saturation are related by a power law (−Ford and Williams, 2007; Bögli, 1964). However, mixing models of UFA waters with different initial pCO_2 showed little to no undersaturation (Gulley et al., 2014). In addition, UFA spring conduits commonly have dissolution scallops on walls indicating formation by water flowing into the spring system during reversals (Gulley et al., 2011). Dissolution resulting from mixing UFA waters in spring conduits, which would occur most frequently during baseflow conditions, would not produce dissolution scallops indicating an inward flow direction.

The importance of point surface water-groundwater interactions to dissolution of conduits arises from high primary porosity and permeability of aquifer rock in the eogenetic UFA (e.g., Vacher and Mylroie, 2002; Choquette and Pray, 1970). Diffusely distributed undersaturated recharge into eogenetic karst aquifers equilibrates with calcite during recharge through the vadose zone (e.g., Gabrovšek and Dreybrodt, 2010), limiting dissolution in conduits, which are typically 20–30 m below the water table of the UFA (Brown et al., 2014; Meyerhoff et al., 2012; Moore et al., 2009; Florea et al., 2007). Where eogenetic aquifers are confined, undersaturated stream water can be focused into existing dissolution features as point recharge (Gulley et al., 2013b) and undersaturation would be enhanced by acid generated from redox reactions (Tables 1 and 4). In contrast with eogenetic aquifers, little dissolution occurred during spring reversals in the telogenetic Mammoth Cave Karst Aquifer (Kentucky, USA) because low bulk permeability of the carbonate rock focused flow, limited conduit-matrix exchange and caused short subsurface residence time (Kipper, 2019). Contrasting hydrogeologic properties of the UFA and the Mammoth Cave Karst Aquifer highlights how characteristics of karst aquifer, and their impacts on the residence time of undersaturated water in the subsurface, may be more critical to development of secondary porosity than the degree of water undersaturation.

Although aquifer characteristics contribute to dissolution effects of recharging water, our results are relevant to dissolution across other karst systems. Our findings show that enhanced dissolution potential from acid produced through changes in subsurface redox conditions may be significant to a range of epigenetic (telogenetic and eogenetic, inland and coastal) karst systems (e.g., Binet et al., 2022; Gulley et al., 2020; Gulley et al., 2016; Gulley et al., 2015; Kipper, 2019; Cooper et al., 2016; Albéric and Lepiller, 1998). In addition, because of rapid kinetics of redox reactions and slower dissolution kinetics, variation in subsurface residence time is an important control on dissolution during surface water-groundwater interactions in carbonate aquifers (e.g., Oberhelman et al., 2024).

5. Conclusions

Our results indicate that carbonic, sulfuric, and nitric acids produced by redox reactions during surface water-groundwater interactions in an

eogenetic carbonate aquifer may cause as much dissolution as can be attributed to the initial undersaturation of recharged surface waters. Mass balance estimates of electron acceptors and donors indicate that both aerobic and anerobic redox reactions contribute acid despite persistent aerobic conditions at spring vents. Stoichiometry of carbonate mineral dissolution by nitric and sulfuric acids indicates a net release of CO_2 to the atmosphere. The magnitude of the release depends on the frequency of surface water-groundwater interactions across the carbonate critical zone. The rate of calcite dissolution during point surface water-groundwater interactions shows that depending on the morphology of the conduit system, the subsurface residence time of recharged surface water is a more important control on total dissolution than the volume of surface water recharged and its saturation state. These point surface water-groundwater interactions are responsible for most of the dissolution in this partially confined eogenetic carbonate aquifer. Dissolution by redox-related acids in teleogenetic carbonate aquifers are less well defined and may be limited by shorter residence times and little exchange of water between conduits and matrix porosity. Nonetheless, acid produced by redox reactions, and their links to surface water-groundwater interactions are important to conduit development and carbon cycling in the carbonate critical zone.

CRediT authorship contribution statement

Andrew Oberhelman: Writing – review & editing, Writing – original draft, Project administration, Methodology, Investigation, Funding acquisition, Formal analysis, Data curation, Conceptualization. **Jonathan B. Martin:** Writing – review & editing, Methodology, Investigation, Funding acquisition. **Madison K. Flint:** Writing – review & editing, Project administration, Methodology, Investigation.

Declaration of competing interest

The authors declare no conflicts of interest.

Data availability

The data are available on HydroShare (Oberhelman et al., 2023a).

Acknowledgements

This work was supported by grants from the Cave Research Foundation, the University of Florida, and the National Science Foundation (EAR-1905259). We are grateful for permission to sample springs from the Florida Department of Environmental Protection (permit number 08122212) and the assistance of personnel at Florida State Parks and the Suwannee River Water Management District. Thanks to Alex Janelle and Adrian Barry-Sosa for assistance with field work and to Jason Curtis, George Kamenov, and Ray Thomas for assistance with sample analysis.

Appendix A. Supplementary data

Supplementary data to this article can be found online at https://doi.org/10.1016/j.chemgeo.2024.122229.

References

Agnew, R.J., Halihan, T., 2018. Why Springs Bubble: a framework for gas discharge in groundwater. Groundwater 56 (6), 859–870. https://doi.org/10.1111/gwat.12789.

Albéric, P., Lepiller, M., 1998. Oxydation de la matière organique dans un système hydrologique karstique alimenté par des pertes fluviales (Loiret, France)oxidation of organic matter in a karstic hydrologic unit supplied through stream sinks (Loiret, france). Water Res. 32 (7), 2051–2064. https://doi.org/10.1016/s0043-1354(97)00439-9.

Anderson, S.P., Drever, J.I., Frost, C.D., Holden, P., 2000. Chemical weathering in the foreland of a retreating glacier. Geochim. Cosmochim. Acta 64 (7), 1173–1189. https://doi.org/10.1016/s0016-7037(99)00358-0.

Bailly-Comte, V., Martin, J.B., Jourde, H., Screaton, E., Pistre, S., Langston, A.L., 2010. Water exchange and pressure transfer between conduits and matrix and their influence on hydrodynamics of two karst aquifers with sinking streams. J. Hydrol. 386 (1–4), 55–66. https://doi.org/10.1016/j.jhydrol.2010.03.005.

Bailly-Comte, V., Martin, J.B., Screaton, E., 2011. Time variant cross correlation to assess residence time of water and implication for hydraulics of a sink-rise karst system. Water Resour. Res. 47 (5) https://doi.org/10.1029/2010wr009613.

Baldini, J.U., Baldini, L.M., McDermott, F., Clipson, N., 2006. Carbon dioxide sources, sinks, and spatial variability in shallow temperate zone caves : evidence from Ballynamintra Cave, Ireland. J. Cave Karst Stud. 68 (1), 4–11.

Beaulieu, E., Goddéris, Y., Labat, D., Roelandt, C., Calmels, D., Gaillardet, J., 2011. Modeling of water-rock interaction in the Mackenzie basin: competition between sulfuric and carbonic acids. Chem. Geol. 289 (1–2), 114–123. https://doi.org/10.1016/j.chemgeo.2011.07.020.

Berner, R.A., Lasaga, A.C., Garrels, R.M., 1983. The carbonate-silicate geochemical cycle and its effect on atmospheric carbon dioxide over the past 100 million years. Am. J. Sci. 283 (7), 641–683. https://doi.org/10.2475/ajs.283.7.641.

Binet, S., Charlier, J., Jozja, N., Défarge, C., Moquet, J., 2022. Evidence of long term biogeochemical interactions in carbonate weathering: the role of planktonic microorganisms and riverine bivalves in a large fluviokarst system. Sci. Total Environ. 842, 156823 https://doi.org/10.1016/j.scitotenv.2022.156823.

Bögli, A., 1964. Mischungskorrosion - ein beitrag zum verkarstungsproblem. Erdkunde 18 (2), 83–92. https://doi.org/10.3112/erdkunde.1964.02.02.

Brigmon, R.L., Martin, H.W., Morris, T., Bitton, G., Zam, S.G., 1994. Biogeochemical ecology of Thiothrix spp. in underwater limestone caves. Geomicrobiol J. 12 (3), 141–159. https://doi.org/10.1080/01490459409377982.

Brown, A.L., Martin, J.B., Screaton, E., Ezell, J., Spellman, P., Gulley, J., 2014. Bank storage in karst aquifers: the impact of temporary intrusion of river water on carbonate dissolution and trace metal mobility. Chem. Geol. 385, 56–69. https://doi.org/10.1016/j.chemgeo.2014.06.015.

Brown, A.L., Martin, J.B., Kamenov, G.D., Ezell, J., Screaton, E., Gulley, J., Spellman, P., 2019. Trace metal cycling in karst aquifers subject to periodic river water intrusion. Chem. Geol. 527, 118773 https://doi.org/10.1016/j.chemgeo.2018.05.020.

Budd, D.A., Vacher, H.L., 2004. Matrix permeability of the confined Floridan Aquifer, Florida, USA. Hydrogeol. J. 12 (5), 531–549. https://doi.org/10.1007/s10040-004-0341-5.

Buhmann, D., Dreybrodt, W., 1985. The kinetics of calcite dissolution and precipitation in geologically relevant situations of karst areas: 1. Open system. Chem. Geol. 53 (1–2), 109–124. https://doi.org/10.1016/0009-2541(85)90024-5.

Choquette, P., Pray, L., 1970. Geologic nomenclature and classification of porosity in sedimentary carbonates. AAPG Bull. 54, 207–250. https://doi.org/10.1306/5d25c98b-16c1-11d7-8645000102c1865d.

Cooper, K., Whitaker, F.F., Anesio, A.M., Naish, M., Reynolds, D.M., Evans, E.L., 2016. Dissolved organic carbon transformations and microbial community response to variations in recharge waters in a shallow carbonate aquifer. Biogeochemistry 129 (1–2), 215–234. https://doi.org/10.1007/s10533-016-0226-4.

Covington, M.D., Martin, J.B., Toran, L., Macalady, J.L., Sekhon, N., Sullivan, P.L., Garcia, A.A., Heffernan, J.B., Graham, W.D., 2023. Carbonates in the critical zone. Earth's Future 11 (1). https://doi.org/10.1029/2022ef002765.

Cravotta, C.A., 1993. Secondary iron-sulfate minerals as sources of sulfate and acidity. In: ACS Symposium Series, pp. 345–364. https://doi.org/10.1021/bk-1994-0550.ch023.

de Montety, V., Martin, J., Cohen, M., Foster, C., Kurz, M., 2011. Influence of diel biogeochemical cycles on carbonate equilibrium in a karst river. Chem. Geol. https://doi.org/10.1016/j.chemgeo.2010.12.025.

Engel, A.S., Stern, L.A., Bennett, P.C., 2004. Microbial contributions to cave formation: New insights into sulfuric acid speleogenesis. Geology 32 (5), 369. https://doi.org/10.1130/g20288.1.

Erisman, J.W., Sutton, M.A., Galloway, J.N., Klimont, Z., Winiwarter, W., 2008. How a century of ammonia synthesis changed the world. Nat. Geosci. 1 (10), 636–639. https://doi.org/10.1038/ngeo325.

Falkowski, P.G., Scholes, R.J., Boyle, E., Canadell, J.G., Canfield, D.E., Elser, J.J., Gruber, N., Hibbard, K., Högberg, P., Linder, S., Mackenzie, F.T., Moore, B., Pedersen, T.F., Rosenthal, Y., Seitzinger, S.P., Smetacek, V., Steffen, W., 2000. The global carbon cycle: a test of our knowledge of earth as a system. Science 290 (5490), 291–296. https://doi.org/10.1126/science.290.5490.291.

Ferry, J.G., 2011. Fundamentals of methanogenic pathways that are key to the biomethanation of complex biomass. Curr. Opin. Biotechnol. 22 (3), 351–357. https://doi.org/10.1016/j.copbio.2011.04.011.

Flint, M.K., Martin, J.B., Summerall, T.I., Barry-Sosa, A., Christner, B.C., 2021. Nitrous oxide processing in carbonate karst aquifers. J. Hydrol. 594, 1–13. https://doi.org/10.1016/j.jhydrol.2020.125936.

Florea, L.J., Vacher, H.L., Donahue, B., Naar, D.F., 2007. Quaternary cave levels in peninsular Florida. Quat. Sci. Rev. 26 (9–10), 1344–1361. https://doi.org/10.1016/j.quascirev.2007.02.011.

Ford, D., Williams, P.W., 2007. Karst Hydrogeology and Geomorphology. John Wiley & Sons.

Gabrovšek, F., Dreybrodt, W., 2010. Karstification in unconfined limestone aquifers by mixing of phreatic water with surface water from a local input: a model. J. Hydrol. 386 (1–4), 130–141. https://doi.org/10.1016/j.jhydrol.2010.03.015.

Galloway, J.N., Townsend, A.R., Erisman, J.W., Bekunda, M., Cai, Z., Freney, J.R., Martinelli, L.A., Seitzinger, S.P., Sutton, M.A., 2008. Transformation of the nitrogen cycle: recent trends, questions, and potential solutions. Science 320 (5878), 889–892. https://doi.org/10.1126/science.1136674.

Gao, W., Fan, C., Zhang, W., Li, N., Liu, H., Chen, M., 2023. Heterotrophic nitrification of organic nitrogen in soils: process, regulation, and ecological significance. Biol. Fertil. Soils 59 (3), 261–274. https://doi.org/10.1007/s00374-023-01707-7.
Gu, B., Schmitt, J., Chen, Z., Liang, L., McCarthy, J.F., 1994. Adsorption and desorption of natural organic matter on iron oxide: mechanisms and models. Environ. Sci. Technol. 28 (1), 38–46. https://doi.org/10.1021/es00050a007.
Gulley, J., Martin, J.B., Screaton, E., Moore, P., 2011. River reversals into karst springs: a model for cave enlargement in eogenetic karst aquifers. Geol. Soc. Am. Bull. 123 (3–4), 457–467. https://doi.org/10.1130/b30254.1.
Gulley, J., Martin, J.B., Moore, P., Murphy, J., 2013a. Formation of phreatic caves in an eogenetic karst aquifer by CO_2 enrichment at lower water tables and subsequent flooding by sea level rise. Earth Surf. Process. Landf. 38 (11), 1210–1224. https://doi.org/10.1002/esp.3358.
Gulley, J., Martin, J.B., Spellman, P., Moore, P., Screaton, E., 2013b. Dissolution in a variably confined carbonate platform: effects of allogenic runoff, hydraulic damming of groundwater inputs, and surface-groundwater exchange at the basin scale. Earth Surf. Process. Landf. 38 (14), 1700–1713. https://doi.org/10.1002/esp.3411.
Gulley, J., Martin, J.B., Moore, P., 2014. Vadose CO_2 gas drives dissolution at water tables in eogenetic karst aquifers more than mixing dissolution. Earth Surf. Process. Landf. 39 (13), 1833–1846. https://doi.org/10.1002/esp.3571.
Gulley, J., Martin, J., Moore, P., Brown, A.L., Spellman, P., Ezell, J., 2015. Heterogeneous distributions of CO_2 may be more important for dissolution and karstification in coastal eogenetic limestone than mixing dissolution. Earth Surf. Process. Landf. 40 (8), 1057–1071. https://doi.org/10.1002/esp.3705.
Gulley, J., Martin, J.B., Brown, A.L., 2016. Organic carbon inputs, common ions and degassing: rethinking mixing dissolution in coastal eogenetic carbonate aquifers. Earth Surf. Process. Landf. 41 (14), 2098–2110. https://doi.org/10.1002/esp.3975.
Gulley, J., Breecker, D.O., Covington, M.D., Cooperdock, S., Banner, J.L., Moore, P., Noronha, A., Breithaupt, C., Martin, J.B., Jenson, J.W., 2020. Tidal pumping and biogeochemical processes: dissolution within the tidal capillary fringe of eogenetic coastal carbonates. Earth Surf. Process. Landf. 45 (11), 2675–2688. https://doi.org/10.1002/esp.4922.
Guo, Y., Song, C., Wan, Z., Lü, Y., Qiao, T., Tan, W., Wang, L., 2015. Dynamics of dissolved organic carbon release from a permafrost wetland catchment in Northeast China. J. Hydrol. 531, 919–928. https://doi.org/10.1016/j.jhydrol.2015.10.008.
He, X., Zhou, H., Wan, J., Zhao, H., He, S., 2022. A method for quantifying the role of carbonic acid, sulfuric acid, and nitric acid in carbonate weathering after accounting for the effects of evaporites in the Qingjiang karst catchment. Environ. Earth Sci. 81 (19) https://doi.org/10.1007/s12665-022-10605-4.
Hem, J.D., 1981. Rates of manganese oxidation in aqueous systems. Geochim. Cosmochim. Acta 45 (8), 1369–1374. https://doi.org/10.1016/0016-7037(81)90229-5.
Hessen, D.O., Tranvik, L.J., 1998. Aquatic humic substances. Ecol. Stud. https://doi.org/10.1007/978-3-662-03736-2.
Huang, Q., Qin, X., Liu, P., Zhang, L., Su, C., 2017. Impact of sulfuric and nitric acids on carbonate dissolution, and the associated deficit of CO_2 uptake in the upper–middle reaches of the Wujiang River, China. J. Contam. Hydrol. 203, 18–27. https://doi.org/10.1016/j.jconhyd.2017.05.006.
Irwin, J., Williams, M., 1988. Acid rain: chemistry and transport. Environ. Pollut. 50 (1–2), 29–59. https://doi.org/10.1016/0269-7491(88)90184-4.
Jin, J., Zimmerman, A.R., 2010. Abiotic interactions of natural dissolved organic matter and carbonate aquifer rock. Appl. Geochem. 25 (3), 472–484. https://doi.org/10.1016/j.apgeochem.2009.12.012.
Jones, D.S., Albrecht, H.L., Dawson, K.S., Schaperdoth, I., Freeman, K.H., Pi, Y., Pearson, A., Macalady, J.L., 2012. Community genomic analysis of an extremely acidophilic sulfur-oxidizing biofilm. ISME J. 6 (1), 158–170. https://doi.org/10.1038/ismej.2011.75.
Jones, D.S., Schaperdoth, I., Macalady, J.L., 2014. Metagenomic evidence for sulfide oxidation in extremely acidic cave biofilms. Geomicrobiol J. 31 (3), 194–204. https://doi.org/10.1080/01490451.2013.834008.
Jones, D.S., Polerecký, L., Galdenzi, S., Dempsey, B.A., Macalady, J.L., 2015. Fate of sulfide in the Frasassi cave system and implications for sulfuric acid speleogenesis. Chem. Geol. 410, 21–27. https://doi.org/10.1016/j.chemgeo.2015.06.002.
Kaiser, K., & Guggenberger, G. (2003). Mineral surfaces and soil organic matter. Eur. J. Soil Sci., 54(2), 219–236. doi: 10.1046/j.1365-2389.2003.00544.x.
Katz, B.G., Böhlke, J.K., Hornsby, H.D., 2001. Timescales for nitrate contamination of spring waters, northern Florida, USA. Chem. Geol. 179 (1–4), 167–186. https://doi.org/10.1016/S0009-2541(01)00321-7.
Kipper, C., 2019. Influence of Spring Flow Reversals on Cave Dissolution in a Influence of Spring Flow Reversals on Cave Dissolution in a Telogenetic Karst Aquifer, Mammoth Cave, KY Telogenetic Karst Aquifer, Mammoth Cave, KY [MS Thesis]. Western Kentucky University.
Klimchouk, A., 2016. The Karst paradigm: changes, trends and perspectives. Acta Carsol. 44 (3) https://doi.org/10.3986/ac.v44i3.2996.
Lalonde, K., Mucci, A., Ouellet, A., Gélinas, Y., 2012. Preservation of organic matter in sediments promoted by iron. Nature 483 (7388), 198–200. https://doi.org/10.1038/nature10855.
Li, S., Calmels, D., Han, G., Gaillardet, J., Liu, C., 2008. Sulfuric acid as an agent of carbonate weathering constrained by δ13CDIC: examples from Southwest China. Earth Planet. Sci. Lett. 270 (3–4), 189–199. https://doi.org/10.1016/j.epsl.2008.02.039.
Liu, Z., Dreybrodt, W., 2015. Significance of the carbon sink produced by H 2 O–carbonate–CO_2 –aquatic phototroph interaction on land. Sci. Bull. 60 (2), 182–191. https://doi.org/10.1007/s11434-014-0682-y.
Liu, Z., Dreybrodt, W., Wang, H., 2010. A new direction in effective accounting for the atmospheric CO_2 budget: considering the combined action of carbonate dissolution, the global water cycle and photosynthetic uptake of DIC by aquatic organisms. Earth Sci. Rev. 99 (3–4), 162–172. https://doi.org/10.1016/j.earscirev.2010.03.001.
Liu, Z., Dreybrodt, W., Liu, H., 2011. Atmospheric CO2 sink: silicate weathering or carbonate weathering? Appl. Geochem. 26, S292–S294. https://doi.org/10.1016/j.apgeochem.2011.03.085.
Lu, P., Zhang, G., Apps, J., Zhu, C., 2022. Comparison of thermodynamic data files for PHREEQC. Earth Sci. Rev. 225, 103888 https://doi.org/10.1016/j.earscirev.2021.103888.
Martin, H.W., 1990. Phreatite: a speleothem formed in phreatic limestone conduits. Underw. Speleol. 17 (6), 6–10.
Martin, J.B., 2017. Carbonate minerals in the global carbon cycle. Chem. Geol. 449, 58–72. https://doi.org/10.1016/j.chemgeo.2016.11.029.
Martin, J.B., Dean, R.W., 1999. Temperature as a natural tracer of short residence times for groundwater in karst aquifers. In: Palmer, A.N., Palmer, M.V., Sasowsky, I.D. (Eds.), Special Publication 5: Karst Modeling. Karst Waters Institute, pp. 236–242.
Martin, J.B., Dean, R.W., 2001. Exchange of water between conduits and matrix in the Floridan aquifer. Chem. Geol. 179 (1–4), 145–165. https://doi.org/10.1016/s0009-2541(01)00320-5.
Martin, J.B., Gordon, S.L., 2000. Surface and ground water mixing, flow paths, and temporal variation in chemical compositions of karst springs. In: Sasowsky, I.D., Wicks, C.M. (Eds.), Groundwater Flow and Contaminant Transport in Carbonate Aquifers. A.A. Balkema, Rotterdam, pp. 65–92.
Martin, J.M., Screation, E.J., Martin, J.B., 2006. Monitoring well responses to karst conduit head fluctuations: Implications for fluid exchange and matrix transmissivity in the Floridan aquifer. In: Harmon, R.S., Wicks, C.M. (Eds.), Perspectives on Karst Geomorphology, Hydrology, and Geochemistry - A Tribute Volume to Derek C. Ford and William B. White. Geological Society of America, pp. 209–217. https://doi.org/10.1130/2006.2404(17).
Martin, J.B., Brown, A., Ezell, J., 2013. Do carbonate karst terrains affect the global carbon cycle? Acta Carsol. 42 (2–3) https://doi.org/10.3986/ac.v42i2-3.660.
Matocha, C.J., Dhakal, P., Pyzola, S., 2012. The role of abiotic and coupled biotic/abiotic mineral controlled redox processes in nitrate reduction. In: Advances in Agronomy, pp. 181–214. https://doi.org/10.1016/b978-0-12-394276-0.00004-4.
Mattey, D., Atkinson, T., Barker, J., Fisher, R., Latin, J., Durrell, R., Ainsworth, M., 2016. Carbon dioxide, ground air and carbon cycling in Gibraltar karst. Geochim. Cosmochim. Acta 184, 88–113. https://doi.org/10.1016/j.gca.2016.01.041.
Mattson, M.D., Likens, G.E., 1993. Redox reactions of organic matter decomposition in a soft water lake. Biogeochemistry 19 (3). https://doi.org/10.1007/bf00000876.
McMahon, P.B., Belitz, K., Barlow, J.R.B., Jurgens, B.C., 2017. Methane in aquifers used for public supply in the United States. Appl. Geochem. 84, 337–347. https://doi.org/10.1016/j.apgeochem.2017.07.014.
Meinzer, O.E., 1927. Large Springs in the United States, Water Supply Paper 557. Unites States Geological Survey. https://doi.org/10.3133/wsp557.
Meyerhoff, S.B., Karaoulis, M., Fiebig, F., Maxwell, R.M., Revil, A., Martin, J.B., Graham, W.D., 2012. Visualization of conduit-matrix conductivity differences in a karst aquifer using time-lapse electrical resistivity. Geophys. Res. Lett. 39 (24) https://doi.org/10.1029/2012gl053933.
Moore, P.J., Martin, J.B., Screaton, E.J., 2009. Geochemical and statistical evidence of recharge, mixing, and controls on spring discharge in an eogenetic karst aquifer. J. Hydrol. 376 (3–4), 443–455. https://doi.org/10.1016/j.jhydrol.2009.07.052.
Moore, P., Martin, J.B., Screaton, E.J., Neuhoff, P.S., 2010. Conduit enlargement in an eogenetic karst aquifer. J. Hydrol. 393 (3–4), 143–155. https://doi.org/10.1016/j.jhydrol.2010.08.008.
Newton, R.M., Burns, D.A., Blette, V.L., Driscoll, C.T., 1996. Effect of whole catchment liming on the episodic acidification of two adirondack streams. Biogeochemistry 32 (3), 299–322. https://doi.org/10.1007/bf02187143.
Oberhelman, A., Martin, J.B., Flint, M., 2023a. Water chemistry and FDOM data from North-Central Florida springs and wells. HydroShare. https://doi.org/10.4211/hs.59786af26dd745fd8e07750d128b14ee.
Oberhelman, A., Martin, J.B., Flint, M., 2023b. Methane cycling in the carbonate critical zone. Sci. Total Environ. 899, 165645 https://doi.org/10.1016/j.scitotenv.2023.165645.
Oberhelman, A., Martin, J.B., Flint, M., 2024. Groundwater-surface water interaction, dissolved organic carbon oxidation and dissolution in carbonate aquifers. Earth Surf. Process. Landforms Early View 1–15. https://doi.org/10.1002/esp.5830.
Parkhurst, D.L., Appelo, C.A.J., 2013. Description of Input and Examples for PHREEQC Version 3: A Computer Program for Speciation, Batch-Reaction, One-Dimensional Transport, and Inverse Geochemical Calculations (Techniques and Methods 6-A43). U.S. Geological Survey. https://doi.org/10.3133/tm6A43.
Perrin, A., Probst, A., Probst, J., 2008. Impact of nitrogenous fertilizers on carbonate dissolution in small agricultural catchments: implications for weathering CO_2 uptake at regional and global scales. Geochim. Cosmochim. Acta 72 (13), 3105–3123. https://doi.org/10.1016/j.gca.2008.04.011.
Pichler, T., Price, R.E., Lazareva, O., Dippold, A.C., 2011. Determination of arsenic concentration and distribution in the Floridan Aquifer System. J. Geochem. Explor. 111 (3), 84–96. https://doi.org/10.1016/j.gexplo.2011.02.004.
Price, R.E., Pichler, T., 2006. Abundance and mineralogical association of arsenic in the Suwannee Limestone (Florida): implications for arsenic release during water–rock interaction. Chem. Geol. 228 (1–3), 44–56. https://doi.org/10.1016/j.chemgeo.2005.11.018.
Ritorto, M., Screaton, E.J., Martin, J.B., Moore, P.J., 2009. Relative importance and chemical effects of diffuse and focused recharge in an eogenetic karst aquifer: an example from the unconfined upper Floridan aquifer, USA. Hydrogeol. J. 17 (7), 1687–1698. https://doi.org/10.1007/s10040-009-0460-0.
Schmidt, W., Hoenstine, R.W., Knapp, M.S., Lane, E., Ogden, G.M., Scott, T.M., 1979. The limestone, dolomite and coquina resources of Florida. In: Report of Investigation 88.

Bureau of Geology, Division of Resource Management, Florida Department of Natural Resources, Tallahassee, Florida.
Scott, T.M., 1988. The Lithostratigraphy of the Hawthorn Group (Miocene) of Florida (FGS: Bulletin 59). Florida Geological Survey. https://ufdc.ufl.edu/UF00000226/00001.
Screaton, E., Martin, J.B., Ginn, B.K., Smith, L.C., 2004. Conduit properties and karstification in the unconfined Floridan aquifer. Ground Water 42 (3), 338–346. https://doi.org/10.1111/j.1745-6584.2004.tb02682.x.
Stein, L.Y., 2011. Heterotrophic nitrification and nitrifier denitrification. In: ASM Press eBooks, pp. 95–114. https://doi.org/10.1128/9781555817145.ch5.
Suwannee River Water Management District, 2024. Real-Time Rainfall: Current Rainfall Amounts. Accessed May 1, 2024, from. http://www.mysuwanneeriver.org/realtime/rain-levels.php.
Torres, M.A., West, A.J., Li, G., 2014. Sulphide oxidation and carbonate dissolution as a source of CO_2 over geological timescales. Nature 507 (7492), 346–349. https://doi.org/10.1038/nature13030.
Vacher, H.L., Mylroie, J.E., 2002. Eogenetic karst from the perspective of an equivalent porous medium. Carbonates Evaporites 17 (2), 182–196. https://doi.org/10.1007/bf03176484.
Walker, J.C.G., Hays, P.B., Kasting, J.F., 1981. A negative feedback mechanism for the long-term stabilization of Earth's surface temperature. J. Geophys. Res. 86 (C10), 9776–9782. https://doi.org/10.1029/jc086ic10p09776.
Wang, X., Sun, G., Zhu, Y., 2017. Thermodynamic energy of anaerobic microbial redox reactions couples elemental biogeochemical cycles. J. Soils Sediments 17 (12), 2831–2846. https://doi.org/10.1007/s11368-017-1767-4.
Whitaker, F.F., Smart, P.L., 2007. Geochemistry of meteoric diagenesis in carbonate islands of the northern Bahamas: 1. Evidence from field studies. Hydrol. Process. 21 (7), 949–966. https://doi.org/10.1002/hyp.6532.
Williams, L.J., Kuniansky, E.L., 2015. Revised Hydrogeologic Framework of the Floridan Aquifer System in Florida and Parts of Georgia, Alabama, and South Carolina. U.S. Geological Survey Professional Paper. https://doi.org/10.3133/pp1807.
Wood, W.W., 1985. Origin of caves and other solution openings in the unsaturated (vadose) zone of carbonate rocks: a model for CO_2 generation. Geology 13 (11), 822. https://doi.org/10.1130/0091-7613(1985)13.
Xie, Y., Huang, F., Yang, H., Yu, S., 2021. Role of anthropogenic sulfuric and nitric acids in carbonate weathering and associated carbon sink budget in a karst catchment (Guohua), southwestern China. J. Hydrol. 599, 126287 https://doi.org/10.1016/j.jhydrol.2021.126287.
Zhang, Y., Jiang, Y., Yuan, D., Cui, J., Li, Y., Yang, J., Cao, M., 2020. Source and flux of anthropogenically enhanced dissolved inorganic carbon: a comparative study of urban and forest karst catchments in Southwest China. Sci. Total Environ. 725, 138255 https://doi.org/10.1016/j.scitotenv.2020.138255.